Physics and characteristics of high performance 1200 nm InGaAs and 1300–1400 nm InGaAsN quantum well lasers obtained by metal–organic chemical vapour deposition

2004 J. Phys.: Condens. Matter 16 S3277

(http://iopscience.iop.org/0953-8984/16/31/020)

INSTITUTE OF PHYSICS PUBLISHING JOURNAL OF PHYSICS: CONDENSED MATTER

J. Phys.: Condens. Matter **16** (2004) S3277–S3318 PII: S0953-8984(04)77707-3

Physics and characteristics of high performance 1200 nm InGaAs and 1300–1400 nm InGaAsN quantum well lasers obtained by metal–organic chemical vapour deposition

Nelson Tansu[1], **Jeng-Ya Yeh**[2] **and Luke J Mawst**[2]

[1] Center for Optical Technologies, Department of Electrical and Computer Engineering, Lehigh University, Sinclair Laboratory, 7 Asa Drive, Bethlehem, PA 18015, USA
[2] Reed Center for Photonics, Department of Electrical and Computer Engineering, University of Wisconsin-Madison, 1415 Engineering Drive, Madison, WI 53706, USA

E-mail: Tansu@Lehigh.Edu

Received 11 March 2004, in final form 7 June 2004
Published 23 July 2004
Online at stacks.iop.org/JPhysCM/16/S3277
doi:10.1088/0953-8984/16/31/020

Abstract

Here we present the physics and device characteristics of high performance strain-compensated MOCVD-grown 1200 nm InGaAs and 1300–1400 nm InGaAsN quantum well (QW) lasers. Utilizing the GaAsP barriers surrounding the highly strained InGaAsN QW active regions, high performance QW lasers have been realized from 1170 nm up to 1400 nm wavelength regions. The design of the InGaAsN QW active region utilizes an In content of approximately 40%, which requires only approximately 0.5–1% N content to realize emission wavelengths up to 1300–1410 nm. Threshold current densities of only 65–90 A cm^{-2} were realized for InGaAs QW lasers, with emission wavelengths of 1170–1233 nm. Room temperature threshold and transparency current densities of 210 and 75–80 A cm^{-2}, respectively, have been realized for 1300 nm InGaAsN QW lasers. Despite the utilization of the highly strained InGaAsN QW, multiple-QW lasers have been realized with excellent lasing performance. Methods for extending the lasing emission wavelength up to 1400 nm with InGaAsN QW lasers are also presented. Theoretical analysis and experiments also show suppression of thermionic carrier leakages in InGaAsN QW systems leading to high performance lasers operating at high temperature.

(Some figures in this article are in colour only in the electronic version)

1. Introduction

The demand for higher bandwidth and longer transmission distance has led to the pursuit of low cost single-mode 1300–1550 nm transmitter sources. Transmitters based on 1300 nm edge emitters or vertical-cavity surface emitting lasers (VCSELs) operating at a modulation bandwidth of 10 Gb s^{-1}, for metro application using single-mode fibre, allow data transmission up to a distance of 20–30 km [1, 2]. In order to realize low cost (uncooled) 1300–1550 nm wavelength-based optical communications systems, high performance (i.e. temperature insensitive) diode lasers (either in-plane or VCSELs) which operate up to 85 °C are needed. However, conventional InP-based long wavelength diode lasers, at $\lambda = 1300$–1550 nm, are inherently highly temperature sensitive, due to strong Auger recombination, large carrier leakage from the active layer, intervalence band absorption, and a strongly temperature dependent material gain parameter [1, 2].

Another major factor motivating the development of 1.3–1.55 μm GaAs-based diode lasers is the ease of forming high quality (Al)GaAs/AlAs distributed Bragg reflectors (DBRs) on GaAs substrates [1, 2]. The ability to fabricate very high quality AlGaAs-based DBRs has allowed the development of GaAs-based VCSELs with performance comparable to that of GaAs-based in-plane diode lasers.

An attractive approach for achieving long wavelength laser emission on GaAs substrates is that using highly strained InGaAsN [1–19] or InGaAs [20–27] QWs. The use of a highly strained InGaAs QW active layer to extend the emission wavelength to 1.20 μm was pioneered by Sato and Satoh [20] and Kondo *et al* [22]. The reduction in the band-gap of the InGaAsN materials achieved due to the incorporation of the N, as pioneered by Kondow *et al* [1], is also followed by reduction in the compressive strain of the material due to the smaller native lattice constant of the InGaN compound. Since then, many promising results have been demonstrated for 1.3 μm InGaAsN active lasers [1–19].

Similarly to those on 1.3 μm lasers on InP, recent studies on recombination mechanisms in InGaAsN/GaAs lasers, at 1.3 μm, suggest that Auger recombination may also be a dominant recombination process in this material system [28]. Other studies identify the role of carrier leakage as well as the material gain parameter in the device temperature sensitivity [29, 30]. At present, a detailed understanding of recombination mechanisms, the material gains, and carrier leakage in this material system is still lacking.

The early development of InGaAsN QW lasers employed nearly lattice-matched low In content and high N content InGaAsN QW active regions [1, 2]. Because of the smaller native lattice constant of the InGaN compound, the incorporation of N into the compressively strained InGaAs material system can result in a nearly lattice-matched InGaAsN QW. Unfortunately, the performances of the early 1200–1300 nm InGaAsN QW lasers were significantly inferior to those of the N-free InGaAs active lasers as well as the conventional 1300 nm InP-based lasers.

Sato and co-workers, of Ricoh Technologies in Japan, proposed the approach of utilizing very high In content InGaAsN QW active regions [3] grown by metal–organic chemical vapour deposition (MOCVD). The idea proposed was to utilize as high an In content as possible in the InGaAsN QW, such that only a minimum amount of N is required to push the peak emission wavelength to 1300 nm. By utilizing this approach, Sato and co-workers were able to realize 1300 nm InGaAsN QW lasers with reasonable threshold current density of the order of 0.9–1 kA cm^{-2}. Prior to 2001, the best 1300 nm InGaAsN QW lasers in the literature [4] were realized with molecular beam epitaxy (MBE), resulting in superior lasing performance in comparison to that of MOCVD-grown 1300 nm InGaAsN QW lasers [3, 5]. Only recently have MOCVD-grown 1300 nm InGaAsN QW lasers [6–14] been realized with performance comparable to that of the best MBE-grown devices.

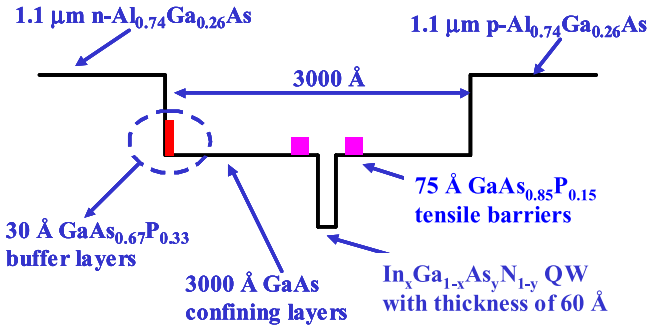

Figure 1. A cross-sectional schematic conduction band diagram of the $In_xGa_{1-x}As_yN_{1-y}$ QW lasers with tensile-strained $GaAs_{0.67}P_{0.33}$ buffer and $GaAs_{0.85}P_{0.15}$ barrier layers.

This paper deals with various aspects of the lasing characteristics of InGaAs QW and InGaAsN QW lasers grown by low pressure MOCVD with AsH_3 as the As precursor. The InGaAs and InGaAsN QW lasers studied here cover emission wavelengths from 1170 up to 1410 nm. The details of the MOCVD growth process and related issues are discussed in section 2. The InGaAsN QW active structures investigated include both single-QW and multiple-QW designs with strain compensation from GaAsP tensile-strained barriers, as discussed in sections 3, 4, and 5. The effect of increased N content on device performance is also discussed in section 6. The first method used to extend the emission wavelength up to 1320 nm, by utilizing GaAsN barriers to reduce the quantum confinement effects of InGaAsN QWs, is discussed in section 7. To clarify the benefits of the InGaAsN QW active region, the comparison with conventional InP technology is also discussed in section 8. Continuous wave lasing characteristics of 1300 nm InGaAsN QW single-mode ridge guide lasers are discussed in section 9. The second method used to extend the emission wavelength of InGaAsN QW lasers up to the 1400 nm region, by utilizing higher N content InGaAsN QW gain media, is discussed in section 10. The temperature analysis of the lasing characteristics of InGaAsN QW lasers with increasing N content is also discussed in section 11. Sections 12 and 13 discuss the theoretical and the experimental evidence, respectively, for the impact of thermionic emission processes on the high temperature lasing performances of InGaAsN QW lasers.

2. MOCVD-grown InGaAs(N) QWs

All the laser structures studied here were grown by low pressure MOCVD. Trimethylgallium (TMGa), trimethylaluminium (TMAl), and trimethylindium (TMIn) are used as the group III sources and AsH_3, PH_3, and U-dimethylhydrazine (U-DMHy) are used as the group V sources. The dopant sources are SiH_4 and dielthylzinc (DEZn) for the n- and p-type dopants, respectively.

A schematic diagram of the laser structure used for both InGaAs and InGaAsN QW active devices is shown in figure 1. The growth of the QW, the barrier regions, and the optical confinement regions is performed at a temperature of 530 °C. The active regions typically consist of InGaAs and InGaAsN QWs with an In content of approximately 40% and thickness of 60 Å. The lower and upper cladding layers of the lasers consist of $Al_{0.74}Ga_{0.26}As$ layers with doping levels of 1×10^{18} cm^{-3} for both the n and p cladding layers, respectively. The growth temperatures of the n- and p-$Al_{0.74}Ga_{0.26}As$ are 775 and 640 °C, respectively. The annealing of the InGaAsN QW is accomplished during the growth of the top cladding layer

at a temperature of 640 °C, with a duration of approximately 27 min. The InGaAsN QW is surrounded by tensile-strained barriers of $GaAs_{0.85}P_{0.15}$, which are spaced by 100 Å on each side of the QW. The tensile-strained buffer layer consists of a 30 Å $GaAs_{0.67}P_{0.33}$, which we found to be crucial for the growth of the highly strained InGaAs(N) QW materials on top of a high Al content lower cladding layer [8, 9].

One of the challenges in growing InGaAsN QWs with an In content of 40% by MOCVD is due to the difficulties in incorporating N into the InGaAs QW, while maintaining a high optical quality film. The low purity of the N precursor used in MOCVD (U-DMHy) is also suspected to be a reason for the low optical quality of MOCVD-grown InGaAsN QWs. In order to incorporate sufficient N into the InGaAsN QW, a very large [DMHy]/V ratio (as high as 0.961 or high) is required. Due to the high cost and the low purity of the DMHy precursor, lowering the [AsH_3]/III ratio to achieve a large [DMHy]/V ratio would be the preferable option over increasing the DMHy flow. A large [DMHy]/V ratio requires the [AsH_3]/III ratio to be rather low. Takeuchi *et al* [7, 26] has demonstrated that the growth of an InGaAs QW ($\lambda = 1200$ nm) with a *very low* [AsH_3]/III ratio is significantly more challenging compared to the case in which tertiary butyl arsine (TBA) is utilized as the As precursor. As the [AsH_3]/III ratio is reduced, the luminescence of the InGaAs QW reduces rapidly for low [AsH_3]/III ratios (below 15–20), which is however required for achieving sufficiently large [DMHy]/V ratios. These challenges have resulted in difficulties in realizing high performance MOCVD-grown InGaAsN QW lasers with AsH_3 as the As precursor until recently [3, 8, 9]. In our approach, the design of the active region is based on strain-compensated InGaAsN QWs, with very high In content ($\sim$40%) and minimum N content ($\sim$0.5%), to achieve 1300 nm emission. Minimum N content in the InGaAsN QW allows us to grow the active region with an optimized AsH_3/III ratio. The growth rates for $In_{0.35}Ga_{0.65}As_{0.992}N_{0.008}$ and $In_{0.4}Ga_{0.6}As_{0.995}N_{0.005}$ QW active regions are approximately 1.182 and 1.278 μm h^{-1}, respectively. The [AsH_3]/III, V/III, and [DMHy]/V ratios for $In_{0.4}Ga_{0.6}As_{0.995}N_{0.005}$ QW (and $In_{0.35}Ga_{0.65}As_{0.992}N_{0.008}$ QW) active regions are kept at approximately 12 (and 13), 403 (and 437), and 0.969 (and also 0.969), respectively.

All our InGaAs QW [23–25] and InGaAsN QW [8–14] lasers utilize strain-compensation techniques that are based on GaAsP tensile barrier layers. The utilization of larger band-gap barrier materials will potentially lead to suppression of thermionic carrier leakage, which will in turn lead to a reduction in the temperature sensitivity of the threshold current density of the lasers, in particular at high temperature operation [38].

3. Lasing characteristics of 1200 nm InGaAs QWs

Kondow and co-workers, of Hitachi, introduced the InGaAsN material system as a new material system with enormous potential for realizing light emitters on GaAs in the wavelength region of interest for optical communications, namely 1300–1550 nm [1]. Unfortunately early InGaAsN QW lasers suffered from poor lasing performance due to the utilization of nearly lattice-matched InGaAsN [1, 2]. Recently, various groups utilizing In contents as high as 30–40% have been able to realize high performance InGaAsN QW lasers in the wavelength region of 1280–1300 nm [3–17].

In our previous work, InGaAsN QW lasers with an In content of 40% and N content of only 0.5% have been realized with threshold current densities of only 210 A cm^{-2} at an emission wavelength of 1295 nm [9]. From studies on InGaAsN QW lasers with In content of 35–43% [8, 14], we also observe a trend toward reduction in the threshold current densities for 1300 nm InGaAsN QW lasers with increasing In content. Therefore, it is extremely important to realize high performance InGaAs QW lasers with very long emission wavelength, such that it requires a minimal amount of N in the QW to push the emission wavelength to 1300 nm.

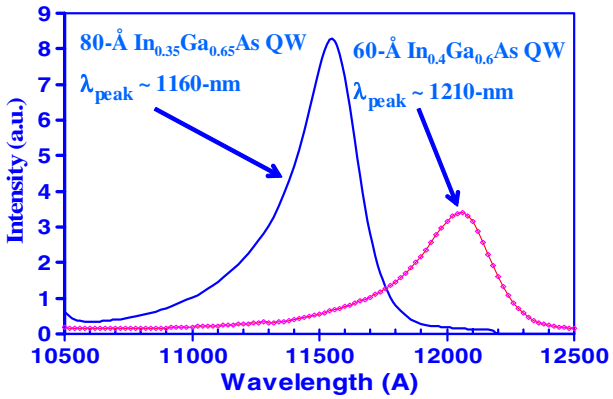

Figure 2. PL spectra of a 1170 nm $In_{0.35}Ga_{0.65}As$ QW and a 1210 nm $In_{0.4}Ga_{0.6}As$ QW.

Here we present high performance InGaAs QW lasers with an emission wavelength beyond 1230 nm, utilizing GaAsP tensile-strained buffer and barrier layers. The high Al content AlGaAs lower cladding layer introduces a slight compressively strained template prior to the growth of the highly strained active region. The tensile-strained GaAsP buffer layer (figure 1) acts to partially strain compensate the QW growth template leading to an improved optical quality for the highly strained InGaAs(N) QW. High optical luminescence intensity from the highly strained InGaAs(N) QW is only obtained with the utilization of the tensile buffer layer [8, 9].

All of the laser structures reported here are realized by low pressure MOCVD. Trimethylgallium (TMGa), trimethylaluminium (TMAl) and trimethylindium (TMIn) are used as the group III sources. The group V precursors used here are AsH_3 and PH_3. The dopant sources are SiH_4 and dielthylzinc (DEZn) for the n and p dopants, respectively. The composition of the QW is characterized by high resolution x-ray diffraction experiments, as has been elaborated in our earlier work [24].

The schematic band diagram of the 1200 nm laser structure is shown as figure 1; this structure is identical to the laser structure previously studied for 1300 nm InGaAsN QW lasers [9] except for the active region. The active region is based on a 60 Å $In_{0.4}Ga_{0.6}As$ QW sandwiched by barrier regions of 100 Å GaAs on each side. The strain compensation of the active region is provided by 75 Å $GaAs_{0.85}P_{0.15}$ tensile barriers, which are grown before and after the GaAs barrier regions. The optical confinement factor for the InGaAs QW is calculated as approximately 1.7%. The growth of the active region and the optical confinement regions utilizes an $[AsH_3]$/III ratio in excess of 100, at a reactor temperature of approximately 530 °C. The n cladding and p cladding layers are based on the $Al_{0.74}Ga_{0.26}As$ material system, and grown at 775 and 640 °C, respectively. Both cladding layers are designed with a doping level of approximately 1×10^{18} cm^{-3}. The tensile buffer layer consists of 30 Å of $GaAs_{0.67}P_{0.33}$, which we found to be crucial for the growth of a highly strained InGaAs(N) QW material system on top of a high Al content lower cladding layer [8, 9].

The room temperature photoluminescence of the 60 Å $In_{0.4}Ga_{0.6}As$ QW active material is presented in figure 2, along with that of an 80 Å $In_{0.35}Ga_{0.65}As$ QW for comparison. The peak emission wavelength of the $In_{0.4}Ga_{0.6}As$ QW is measured at approximately 1210–1215 nm, which is 50–60 nm longer than that of the $In_{0.35}Ga_{0.65}As$ QW. The reduction in the optical luminescence of the $In_{0.4}Ga_{0.6}As$ QW ($\Delta a/a = 2.78\%$), in comparison to that of $In_{0.35}Ga_{0.65}As$ QW ($\Delta a/a = 2.45\%$), is presumably a result of a slight degradation in the crystal quality due to the higher strain of the 1210 nm InGaAs QW.

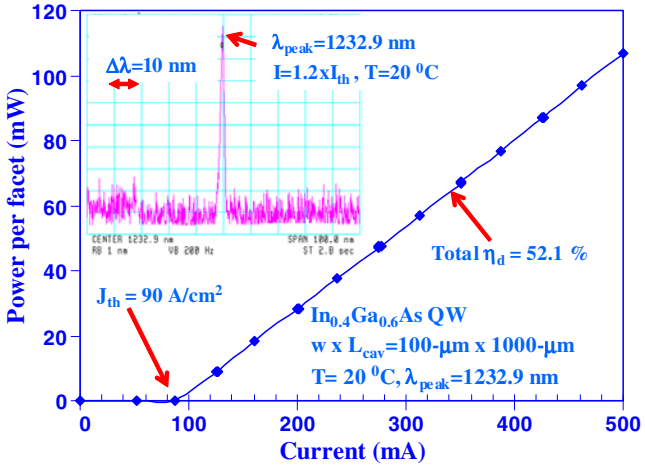

Figure 3. The threshold current density (J_{th}) and external differential quantum efficiency (η_{d}) of 1233 nm $In_{0.4}Ga_{0.6}As$ QW lasers ($L_{\mathrm{cav}} = 1000\ \mu$m) as a function of temperature.

The first step in developing high performance InGaAsN lasers is to establish an optimized growth process for high In content InGaAs active devices operating near the 1200 nm wavelength region. The addition of small quantities (<1%) of nitrogen can then be used to extend the emission wavelength to 1300 nm.

The $In_{0.4}Ga_{0.6}As$ QW laser structure studied here uses strain compensation by $GaAs_{0.85}P_{0.15}$ tensile-strained barriers, as shown in figure 1. The laser utilizes an active region consisting of a 60 Å $In_{0.4}Ga_{0.6}As$ QW. From our earlier studies [8, 9], the existence of a slightly tensile-strained buffer layer is found to be essential for the realization of this laser structure. Broad area lasers with a stripe width of 100 μm are fabricated to characterize the device performance under pulsed conditions (pulse width of 5 μs and duty cycle of 1%). The intrinsic physical device parameters can then be extracted from length dependent studies performed on these lasers.

The room temperature ($T = 20\,^{\circ}$C) lasing spectrum for the 60 Å $In_{0.4}Ga_{0.6}As$ QW devices with cavity lengths of 1000 μm is measured to be at 1233 nm, as shown in figure 3. The lasing emission wavelengths range from 1216 to 1233 nm, with little variation in the threshold current densities (J_{th}). As shown in figure 3, the threshold current densities of these $In_{0.4}Ga_{0.6}As$ QW lasers are found to be 90–92 A cm^{-2} for measurements at a heat sink temperature of 20 °C. The total external differential quantum efficiency (η_{d}) for the devices is measured as approximately 52%.

The temperature characterization of these 1233 nm InGaAs QW lasers, as shown in figure 4, is conducted from a temperature of 10 °C up to a temperature of 10–50 °C, with temperature steps of 5 °C. In the temperature range up to 50 °C, the slope efficiency (η_{d}) hardly decreases with temperature, resulting in a T_1 value ($1/T_1 = (-1/\eta_{\mathrm{d}})\,\mathrm{d}\eta_{\mathrm{d}}/\mathrm{d}T$) of approximately 1250 K based on our best fit. It is important to note that the T_1 values of 1250 K are significantly larger than those of 1300 nm InGaAsN QW lasers. For 1300 nm InGaAsN QW lasers with the same separate confinement heterostructure as the InGaAs active lasers and the cavity length of 1000 μm, we previously reported a T_1 value of 255 K for measurements in the temperature range of 20–60 °C. The T_0 values ($1/T_0 = (1/J_{\mathrm{th}})\,\mathrm{d}J_{\mathrm{th}}/\mathrm{d}T$) are measured as 140 K. These reasonably high T_0 and T_1 values for $In_{0.4}Ga_{0.6}As$ QW lasers result in very

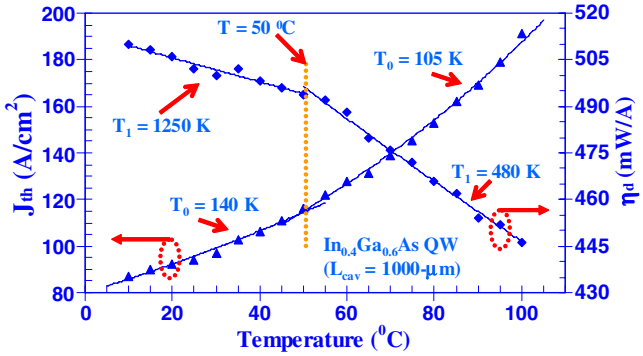

Figure 4. The relation of the output power per facet (P) and the total injected current (I) for $In_{0.4}Ga_{0.6}As$ QW lasers with a cavity length of 1000 μm at a temperature of 20 °C. The inset shows the lasing spectrum at 20 °C.

low threshold current densities of only 160 and 190 A cm^{-2} being achieved for devices with the cavity length of 1000 μm at temperatures of 85 and 100 °C, respectively.

Previously, we have reported room temperature threshold current densities of 65 and 100 A cm^{-2} for InGaAs QW lasers with emission wavelengths of 1170 and 1190 nm, respectively [23, 24]. The transparency current densities for the 1170 and 1190 nm InGaAs QW lasers were measured as 30 and 58 A cm^{-2}, respectively, at room temperature [23, 24]. The material gain parameters (g_{0J}) for both the 1170–1190 nm InGaAs QW lasers had previously been measured as 1600–1900 cm^{-1} [23, 24].

The comparison of the threshold current density ($J_{\rm th}$) for any QW laser is slightly more challenging, and at times could be deceptive when comparing various laser structures. The threshold current density of a QW laser typically depends on various factors, ranging over the quality of the QW active materials, the gain properties of the QWs, the design of the separate confinement heterostructure (SCH) region, the choice of the compositions and doping levels of the cladding layers, and the modal threshold gain. Nevertheless, the comparison of the device performance in terms of threshold current density is still of extreme importance, as this is generally the parameter of practical interest for laser diodes.

A comparison of the threshold current densities of our InGaAs QW lasers with other published results [20–27, 31, 32, 69] is shown in figure 5. The threshold current densities of the 1233 nm $In_{0.4}Ga_{0.6}As$ QW ($L_{\rm cav} = 1000$ μm) and 1170 nm $In_{0.35}Ga_{0.65}As$ lasers ($L_{\rm cav} = 1500$ μm) are approximately 90 and 65 A cm^{-2}, respectively. To the best of our knowledge, these results represent the lowest reported $J_{\rm th}$ values for any QW laser in the wavelength region of 1170–1233 nm. It is also interesting to note that the $J_{\rm tr}$ and $J_{\rm th}$ of approximately 30 and 65 A cm^{-2} for our 1170 nm $In_{0.35}Ga_{0.65}As$ QW lasers are comparable with some of the best reported results realized by quantum dot (QD) active lasers in this wavelength region. The group at the Technical University of Berlin recently reported QD lasers at an emission wavelength of 1.15 μm with $J_{\rm th}$ and $J_{\rm tr}$ of approximately 100 and 20 A cm^{-2}, respectively [33]. The transparency current density in QD lasers is smaller as a result of the smaller active volume of the quantum dots. Although the $J_{\rm tr}$ is smaller, the threshold current density of the QD lasers is not significantly lower than that of the QW laser, because the QD active materials have a low material gain parameter. The relatively low g_0 values of QD active materials as a result of gain saturation lead to modal material gain parameters (Γg_0) of approximately 4.5–9 cm^{-1} per QD stage [34, 35], which are significantly lower than the typical Γg_0 for an InGaAs QW laser ($\Gamma g_0 = 30$–45 cm^{-1} for an InGaAs QW).

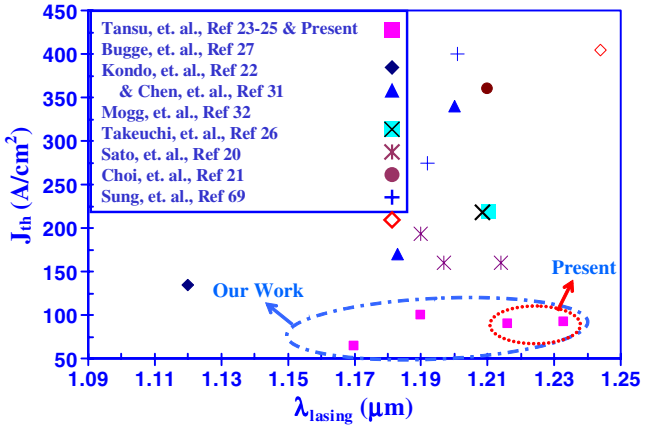

Figure 5. Comparison of J_{th} values for InGaAs QW lasers in the 1100–1250 nm wavelength region.

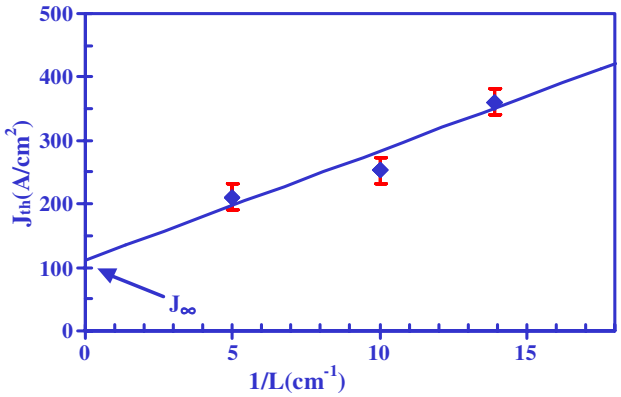

Figure 6. The room temperature J_{th} of the $In_{0.4}Ga_{0.6}As_{0.995}N_{0.005}$–$GaAs_{0.85}P_{0.15}$ QW as functions of the inverse cavity length $(1/L)$.

4. Lasing characteristics of InGaAsN QW lasers

The structure of the InGaAsN laser is shown in figure 1; it is identical to the structure of the InGaAs laser except for the active region. The active region utilized here consists of a 60 Å $In_{0.4}Ga_{0.6}As_{0.995}N_{0.005}$ QW. By utilizing this structure, low threshold (J_{th}) and transparency (J_{tr}) current density, strain-compensated $In_{0.4}Ga_{0.6}As_{0.995}N_{0.005}$ QW lasers with high current injection efficiency (η_{inj}) were realized.

In characterizing the laser performance of the InGaAsN QW, broad area lasers with stripe widths of 100 μm are fabricated. Multi-length studies of various broad area devices, with cavity lengths (L) ranging from 720 to 2000 μm, were utilized to extract the intrinsic device parameters. All the measurements on these broad area devices were performed under pulsed conditions with a pulse width of 6 μs and 1% duty cycle.

The measured threshold current densities, at room temperature (20 °C), for the InGaAsN QW lasers, are shown in figure 6 for various cavity length devices. The threshold and

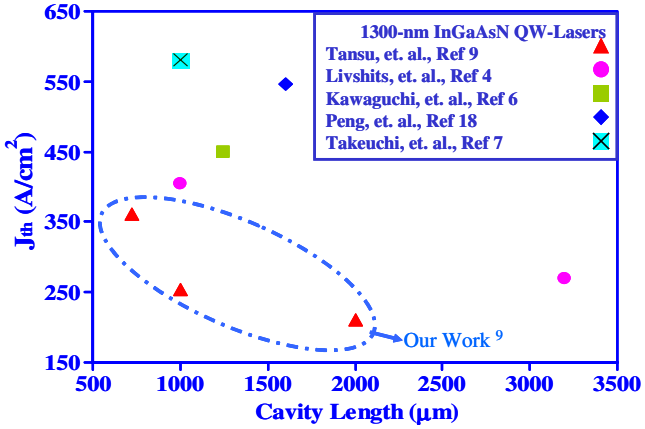

Figure 7. Comparison of the threshold current density versus the cavity length for our 1300 nm InGaAsN QW lasers with those from published results.

Table 1. Threshold current density comparisons for 1300 nm region InGaAsN QW lasers.

References	Growth	L (μm)	J_{th} (A cm^{-2})	J_{tr} (A cm^{-2})	η_d (%)	η_{inj} (%)	α_i (cm^{-1})	λ (μm)	T_0 (K)	T_1 (K)
[4]	MBE	3200	270	110	45	93	4	1.3	75	—
		1000	405	110	70	93	4	1.3	75	—
[17]	MBE	770	1500	—	47	—	—	1.315	65	—
[18]	MBE	1600	546	227	50	80	7	1.317	104	—
[15]	GS-MBE	3000	1150	—	23	82	9.76	1.3	122	—
[5]	MOCVD	800	800		37	75	15	1.28	60	—
[3]	MOCVD	960	920	—	—	—	—	1.29	150	—
[6]	MOCVD	1250	450	—	—	—	—	1.28	205	—
[7]	MOCVD	1000	580	—	—	—	—	1.29	—	—
[8]	MOCVD	750	400	110	51	72	6	1.29	110	416
		1500	289	110	40	72	6	1.295	130	400
[9]	MOCVD	720	361	75	57	97	13	1.29	82	360
		1000	253	75	46	97	13	1.294	88	255
		2000	211	75	33	97	13	1.295	90	200

transparency current densities are measured to be as low as 211 and 79–84 A cm^{-2}, respectively, for devices with the cavity length of 2000 μm, with an emission wavelength of 1.295 μm. Even for shorter cavity devices, 500, 720, and 1000 μm, the threshold current densities are measured to be as low as 450, 361, and 253 A cm^{-2} respectively. To the best of our knowledge, these data represent the *lowest* threshold and transparency current densities reported for InGaAsN QW lasers in the wavelength region of 1.28–1.32 μm, as shown in figure 7 and table 1.

The external differential quantum efficiency (η_d) of the InGaAsN QW lasers is as high as 57% for devices with cavity lengths of 720 μm. The lower η_d for the longer cavity devices is attributed to the relatively large internal loss ($\alpha_i = 10.3$ cm^{-1}) for these unoptimized structures. The internal loss of the lasers may result from the combination of the narrow SCH region and the relatively high doping level (1×10^{18} cm^{-3}) of the p cladding of the laser. By utilizing a thin GaAsP buffer layer in place of the InGaP/GaAsP buffer layer [8], improvement in the current injection efficiency ($\eta_{inj} > 90$–95%) has been achieved as a result of removing the poor interface between the InGaP buffer and GaAs SCH.

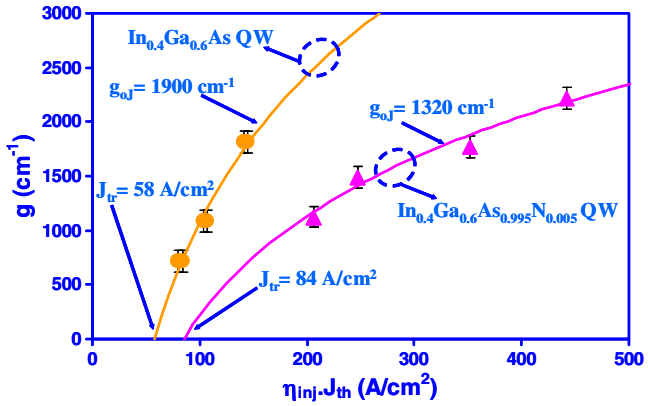

Figure 8. Gain characteristics of InGaAsN QW and InGaAs QW lasers.

The material gain parameter, defined as $g_{0J} = g_{\rm th}/\ln(\eta_{\rm inj}J_{\rm th}/J_{\rm tr})$, is an important parameter in determining the threshold carrier density ($n_{\rm th}$). Low g_{0J} values for a QW laser lead to higher $n_{\rm th}$. Higher $n_{\rm th}$ will result in the possibility of an increase in Auger recombination, due to the $Cn_{\rm th}^3$ behaviour of the Auger recombination rate. Higher $n_{\rm th}$ will also lead to reduced current injection efficiency, due to a larger recombination in the SCH and carrier leakage out of the QW. The material gain parameter (g_{0J}) and the differential gain ($\mathrm{d}g/\mathrm{d}n$) of the InGaAsN QW have been shown to decrease as nitrogen is introduced into the InGaAs QW [29, 30]. As shown in figure 8, the g_{0J} of the InGaAsN QW laser is measured as approximately 1200–1300 cm^{-1}, which is significantly lower than those (g_{0J} = 1600–1900 cm^{-1}) for similar InGaAs QW lasers [22, 26] at λ = 1170–1190 nm. The InGaAsN active devices, with emission wavelengths of 1.29–1.295 μm, exhibit relatively low temperature sensitivity with T_0 values of 82–90 K for devices with cavity lengths of 720–2000 μm. The T_1 values are measured to be in the range 200–360 K, for devices with L of 720–2000 μm.

The continuous wave (CW) operation characteristics of the InGaAsN QW lasers were measured from laser devices with facet coatings of highly reflective (HR) and anti-reflective (AR) layers. The HR layers consist of three Al_2O_3/Si pairs with reflectivity in excess of 95%, and the AR layer was formed of a single layer of Al_2O_3 with reflectivity estimated to be in the range 7–10%. The devices were mounted junction down on copper heat sinks, and they were measured under CW operation for cavity lengths of 1000–2000 μm at temperatures in the range of 10–100 °C.

The measured CW output power ($P_{\rm out}$) characteristics, as a function of the injected current (I) and the heat sink temperature (T), are shown in figure 9. The CW measurements of the InGaAsN QW lasers are measured up to a temperature of 100 °C, limited by our equipment. The near threshold ($I \sim 1.2I_{\rm th}$) emission wavelengths of the InGaAsN QW lasers with the cavity length of 2000 μm are measured as approximately 1295.2 and 1331 nm, at temperatures of 20 and 100 °C, respectively.

The measured threshold current density of the HR/AR coated InGaAsN QW laser devices under CW operation is very much comparable with that of the as-cleaved InGaAsN QW laser devices with the cavity length of 2000 μm. Despite the large internal loss of our lasers ($\alpha_{\rm i}$ is approximately 13 cm^{-1}), the threshold current density of the lasers with the cavity length of 2000 μm is measured as 210–220 A cm^{-2}, at a temperature of 20 °C under CW operation. At elevated temperatures of 80 and 100 °C, the threshold current densities of the HR/AR coated

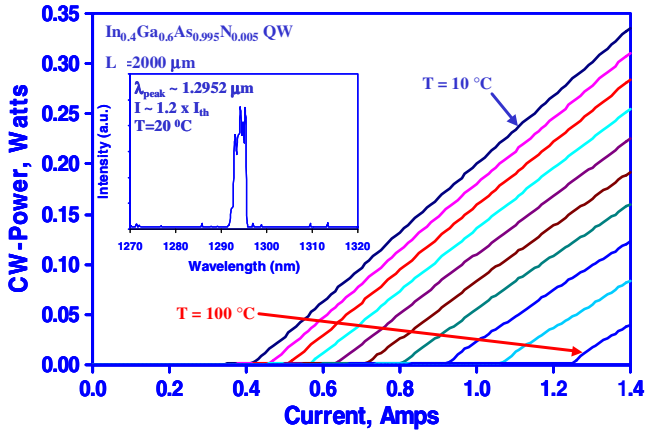

Figure 9. The CW P–I characteristic and spectrum of an InGaAsN laser with $L_{\mathrm{cav}} = 2000\ \mu$m, as a function of temperature.

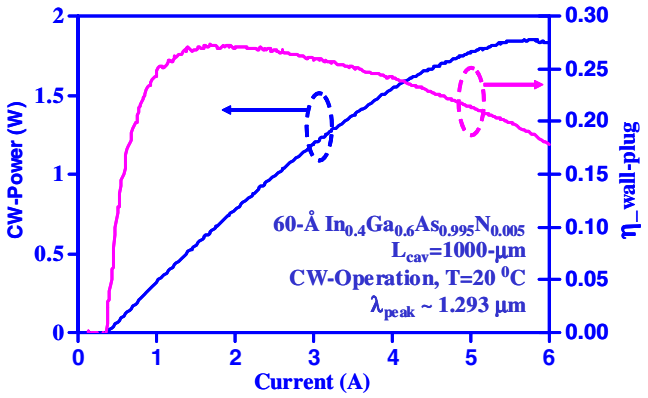

Figure 10. CW output power characteristics for InGaAsN lasers.

($L_{\mathrm{cav}} = 2000\ \mu$m) lasers are measured as only 455 and 615 A cm^{-2}, respectively, under CW operation.

The maximum CW output powers achievable from the 1300 nm InGaAsN QW lasers are approximately 1.8 W for cavity lengths of both 1000 and 2000 μm, at heat sink temperatures of 20 °C. Figure 10 shows the measured output power characteristics for devices with $L_{\mathrm{cav}} = 1000\ \mu$m. This result represents the highest CW output power reported for 1300 nm InGaAsN QW lasers grown by MOCVD at heat sink temperatures of 20 °C. The maximum wall plug efficiency for the cavity length of 1000 μm is approximately 28%, limited by the large internal loss ($\alpha_{\mathrm{i}} = 13\ \mathrm{cm}^{-1}$). Further improvements in the external differential quantum efficiency of InGaAsN QW lasers can be achieved by utilizing a broad waveguide structure to minimize the internal loss.

To compare the lasing performance of the 1300 nm InGaAsN QW lasers with those of the conventional InP technology, we list the published results that represent some of the best performing 1300 nm diode lasers based on conventional InP technology (InGaAsP QW [36] and InGaAlAs QW [37]), as shown in figure 11. Due to the low material gain parameter, carrier leakage, and Auger recombination, typically 1300 nm InGaAsP–InP QW lasers require

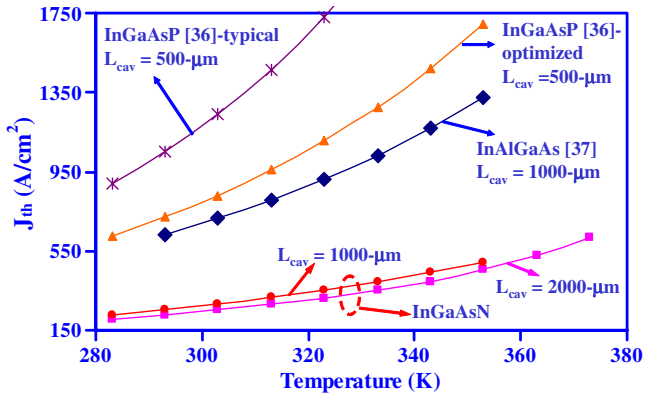

Figure 11. Comparison of J_{th} values for InGaAsN, AlGaInAs, and InGaAsP active lasers as a function of temperature.

multiple QWs, ranging from 9 to 14 QWs [36]. The 1300 nm InGaAlAs QW requires approximately 4–6 QWs for optimized structures [37].

For optimized 1300 nm InGaAsP QW structures, threshold current densities of approximately 1650–1700 A cm^{-2} were achieved for devices with the cavity length of 500 μm at the operation temperature of 80 °C, as reported by Belenky *et al* [36]. The threshold current density of the 1300 nm diode lasers based on the InGaAlAs QW on InP, with the cavity length of 1000 μm, has been reported as approximately 1350 A cm^{-2} at the temperature of 80 °C [37]. The InGaAsN QW lasers require only a single QW active region for high temperature operation, owing to the larger material gain parameter and better electron confinement in the QW. Our 1300 nm InGaAsN single-QW as-cleaved diode lasers, with the cavity lengths of 500 and 1000 μm, have threshold current densities of only 940 and 490 A cm^{-2}, respectively, at the heat sink temperature of 80 °C.

5. 1300 nm InGaAsN multiple-QW lasers

Typically a single QW is sufficient for application in a conventional edge emitting diode laser. There are other types of device which require a structure with multiple QWs as the active region for realizing higher threshold gains and improving the carrier injection efficiency. VCSELs are excellent examples of devices that require higher gain active regions, due to the significantly higher mirror loss in the VCSEL. A concern related to the high In content InGaAs(N) QW is related to the feasibility of implementing multiple-QW layers without material degradation due to the high strain.

The 1300 nm InGaAsN double-QW structure is shown schematically in figure 12. The laser structure studied here consists of a 60 Å InGaAsN double-QW active region, with strain compensation from $GaAs_{0.85}P_{0.15}$ tensile-strained barriers. The optical confinement and the cladding layers of this laser are kept identical to those of the single-QW structure shown in figure 1. Similar to that for the single-QW structure, the thermal annealing of the InGaAsN double-QW structure is conducted at 640 °C for a duration of 27 min.

The room temperature lasing spectrum of the InGaAsN double-QW devices with the cavity length of 1500 μm was measured at 1315 nm with a J_{th} of approximately 410 A cm^{-2}. The slightly longer emission wavelength of the double-QW lasers, in comparison to that of the single-QW lasers, can be attributed to the smaller quasi-Fermi level separation at threshold.

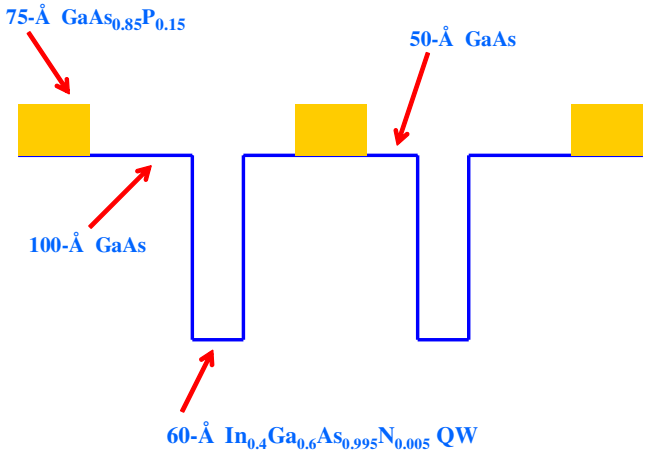

Figure 12. A schematic energy diagram of the active region for the InGaAsN double-QW structures.

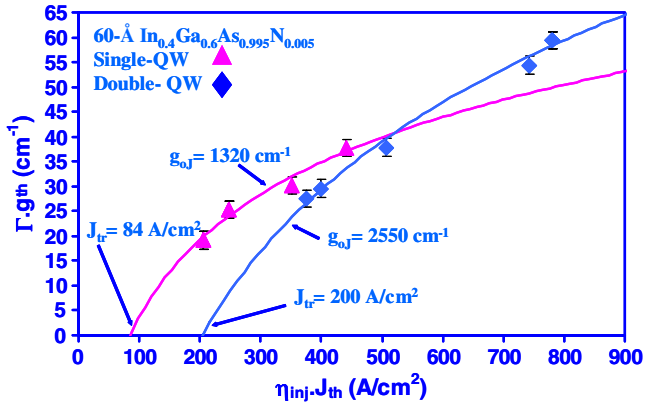

Figure 13. Gain characteristics of the InGaAsN single QW and InGaAsN double QWs.

The J_{tr} and the g_{0J} values for the InGaAsN double-QW lasers are measured as approximately 200 A cm^{-2} and 2520 cm^{-1}, respectively, as shown in figure 13. The scaling of the J_{tr} and g_{0J} values with the number of QWs is in excellent agreement with theory, a good indication of the feasibility of implementing highly strained InGaAsN double-QWs in VCSEL structures.

The 1300 nm InGaAsN triple-QW structure is shown schematically in figure 14. The laser structure studied here consists of a 60 Å InGaAsN triple-QW active region, with strain compensation from $GaAs_{0.85}P_{0.15}$ tensile-strained barriers only surrounding the outer QWs. The optical confinement layer and the cladding layers of this laser are kept identical to those of the single-QW structure shown in figure 1. Similar to those for the single-QW and double-QW structures, the thermal annealing of the InGaAsN triple-QW structure is conducted at 640 °C for a duration of 27 min.

A threshold current density of only 505 A cm^{-2} was achieved for the InGaAsN triple-QW laser devices (L_{cav} = 1000 μm), with the emission wavelength of 1290 nm at room temperature. The measured T_0 values for the triple-QW lasers are approximately 110 K, for measurements in the temperature range of 20–60 °C. The excellent lasing performance of the

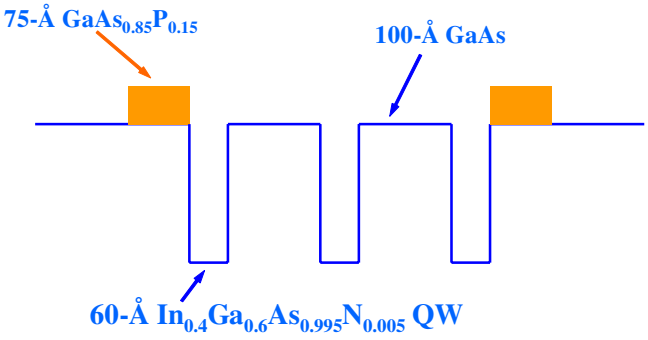

Figure 14. A schematic energy diagram of the active region for the InGaAsN triple-QW structures.

triple-QW structures is a good indication of the feasibility of implementing these triple-QW structures into VCSEL structures.

6. 1300 nm InGaAsN single-QW lasers with higher N content

The lasing characteristics of 1300 nm InGaAsN QW lasers with higher N content are fabricated and analysed for comparison purposes. Higher N content (0.8%) InGaAsN QW lasers are fabricated using lower In content (35%) to keep the emission wavelength fixed at 1300 nm. The thickness of the $In_{0.35}Ga_{0.65}As_{0.992}N_{0.008}$ single-QW structure is adjusted to approximately 80 Å. The In and N compositions are calibrated with secondary-ion mass spectroscopy and x-ray diffraction measurements. In our experiment here, only the active region of the structure, as shown in figure 1, is replaced with an 80 Å $In_{0.35}Ga_{0.65}As_{0.992}N_{0.008}$ single QW. The utilization of a lower In content InGaAsN QW active region allows us to increase the thickness of the QW to 80 Å, which would lead to a reduction of the quantum size effect. The reduced quantum size effect in the lower In content InGaAsN QW will also minimize its N content requirement for achieving a 1300 nm emission wavelength.

The room temperature lasing spectrum of the $In_{0.35}Ga_{0.65}As_{0.992}N_{0.008}$ single-QW devices with the cavity length of 1500 μm was measured at 1305 nm with a J_{th} of approximately 417 A cm^{-2}. As shown in figure 15, the transparency current density of the 1300 nm $In_{0.35}Ga_{0.65}As_{0.992}N_{0.008}$ is estimated as approximately 144 A cm^{-2}, which is almost a factor of two higher in comparison to that of the 1300 nm $In_{0.4}Ga_{0.6}As_{0.995}N_{0.005}$ single QW. Approximately 25% of the increase in its J_{tr} value, in comparison to that of the 60 Å $In_{0.4}Ga_{0.6}As_{0.995}N_{0.005}$ QW, can be attributed to the 25% thicker dimension of the 80 Å $In_{0.35}Ga_{0.65}As_{0.992}N_{0.008}$ QW. The remaining 70–75% increase in the J_{tr} value of $In_{0.35}Ga_{0.65}As_{0.992}N_{0.008}$ QW lasers, in comparison to that of the $In_{0.4}Ga_{0.6}As_{0.995}N_{0.005}$ QW, can be attributed to several other factors including the increase in monomolecular recombination processes, carrier leakage, and other processes. The material gain parameter (g_{0J}) of the $In_{0.35}Ga_{0.65}As_{0.992}N_{0.008}$ QW is measured as 1265 cm^{-1}, as shown in figure 15.

The T_0 and T_1 values of the $In_{0.35}Ga_{0.65}As_{0.992}N_{0.008}$ QW lasers are found to be significantly lower in comparison to those of the $In_{0.4}Ga_{0.6}As_{0.995}N_{0.005}$ QW lasers, as shown in figures 16 and 17, respectively. T_0 and T_1 values of only 75–80 and 100–150 K, respectively, are measured for $In_{0.35}Ga_{0.65}As_{0.992}N_{0.008}$ QW lasers with cavity lengths from 750 to 1500 μm. Careful studies are still required to clarify the mechanisms that lead to the lower T_0 values in these higher N content InGaAsN QW lasers, in spite of their higher J_{th}. Possible mechanisms leading

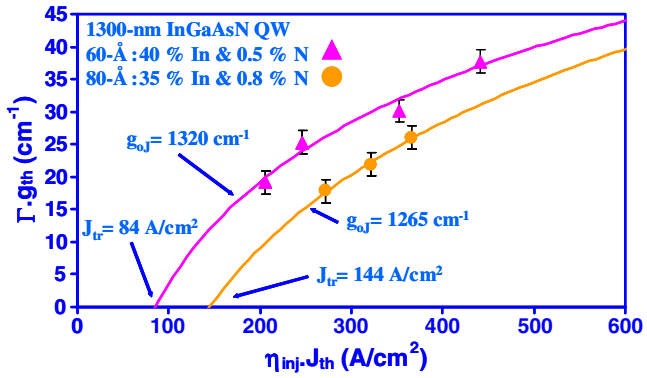

Figure 15. Gain characteristics of the 60 Å $In_{0.4}Ga_{0.6}As_{0.995}N_{0.005}$ single QW and the 80 Å $In_{0.35}Ga_{0.65}As_{0.992}N_{0.008}$ single QW.

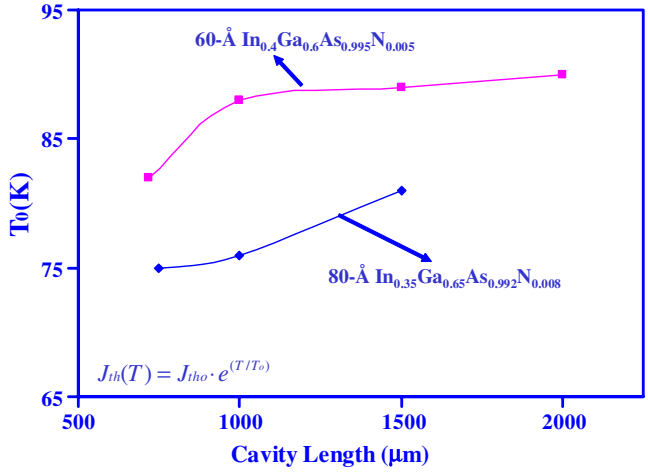

Figure 16. The T_0 comparison for 80 Å $In_{0.35}Ga_{0.65}As_{0.992}N_{0.008}$ single-QW and 60 Å $In_{0.4}Ga_{0.6}As_{0.995}N_{0.005}$ single-QW lasers, for the temperature range of 20–60 °C.

to the lower T_0 and T_1 values include the increase in carrier leakage resulting from a reduction in the hole confinement for higher N content InGaAsN QW lasers, which would also lead to a more temperature sensitive current injection efficiency.

7. 1320 nm InGaAsN QW lasers with GaAsN barriers

In earlier sections, promising results [4, 6–19] have shown the tremendous potential for InGaAsN QW lasers as an alternative material system to replace the conventional technology in the 1300 nm wavelength region. InGaAsN QW lasers have demonstrated impressive results for devices with emission wavelengths slightly below or at 1300 nm [4, 6–19]. Only a few results for 1300 nm InGaAsN QW lasers with GaAsN barriers, from Stanford University [17] and Tampere University of Technology (Finland) [18, 19], utilizing molecular beam epitaxy (MBE) have been realized with reasonably good lasing performance at emission wavelengths beyond 1315 nm. The utilization of GaAsN barriers surrounding the InGaAsN QW has been pursued

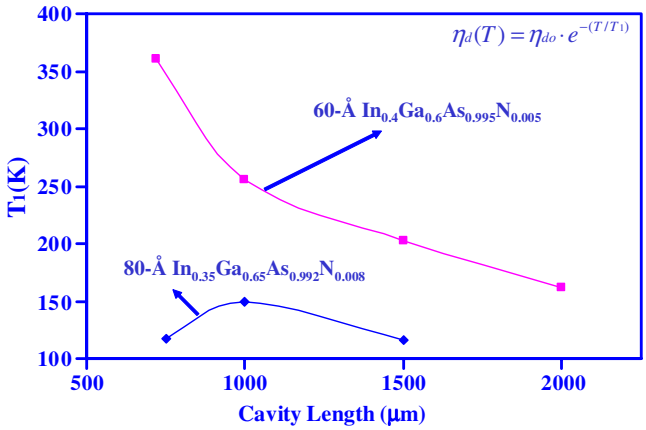

Figure 17. The T_1 comparison for 80 Å $In_{0.35}Ga_{0.65}As_{0.992}N_{0.008}$ single-QW and 60 Å $In_{0.4}Ga_{0.6}As_{0.995}N_{0.005}$ single-QW lasers, for the temperature range of 20–60 °C.

previously by several other groups using MBE technology [17–19]. Most of these efforts had the intention of achieving slightly longer emission wavelength beyond 1300 nm, by reducing the quantum confinement effect. An additional benefit of the utilization of tensile-strained GaAsN barriers is the strain compensation of the highly compressively strained InGaAsN QW.

The method that we pursue here is utilizing InGaAsN QW lasers with GaAsN barriers grown by metal–organic chemical vapour deposition (MOCVD). In addition to a reduction in the quantum confinement effect, we also find improvements in the lasing characteristics at elevated temperatures, presumably as a result of stronger hole confinement.

All the laser structures reported here are realized by low pressure MOCVD, similar to the growth processes and conditions described in section 2. The design of the laser structure is shown in figure 18, with the active region composed of a 60 Å $In_{0.4}Ga_{0.6}As_{0.995}N_{0.005}$ QW surrounded by 35 Å $GaAs_{0.97}N_{0.03}$ tensile-strained barriers on each side. The composition of the InGaAsN QW and GaAsN barriers was determined using high resolution x-ray diffraction and secondary-ion mass spectroscopy. The active region and GaAsN barrier regions are embedded symmetrically inside a 3000 Å undoped GaAs optical confinement region and $Al_{0.74}Ga_{0.26}As$ cladding layers, resulting in an optical confinement factor of 1.7% similar to that of the structure in figure 1. Broad area lasers are fabricated with a stripe width of 100 μm, with structures and fabrication steps similar to those for the laser structures described in earlier sections.

As-cleaved laser devices are characterized under pulsed conditions, with a pulse width of 5 μs and duty cycle of 1%, for various cavity lengths ranging from 750 to 2000 μm at room temperature ($T = 20\,^{\circ}$C). The room temperature ($T = 20\,^{\circ}$C) threshold current density and near threshold lasing spectrum of an InGaAsN–GaAsN QW laser with the cavity length of 750 μm are measured as 300 A cm^{-2} and 1311 nm, respectively, as shown in figure 19. A red-shift of approximately 20–25 nm in emission wavelength was observed for the InGaAsN–GaAsN QW lasers compared to those for our previously reported InGaAsN–GaAs structures [9], resulting in an emission wavelength of 1317 nm for devices with a cavity length of 1500 μm. Threshold current densities (J_{th}) of only 270, 230, and 210 A cm^{-2} are measured for devices with cavity lengths of 1000, 1500, and 2000 μm, respectively. A total external differential quantum efficiency as high as 43–46% (420–430 mW A^{-1}) was also

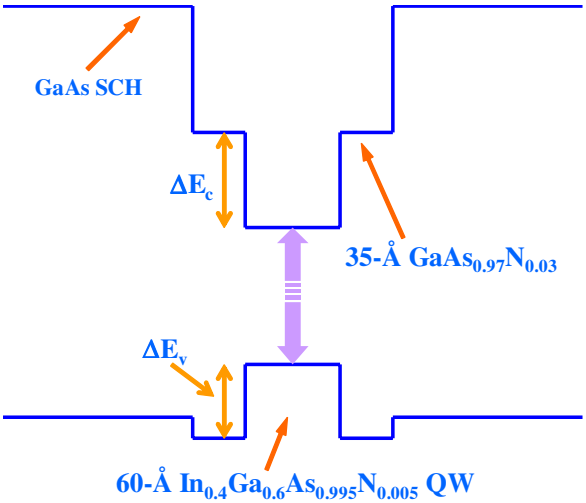

Figure 18. A schematic band diagram of the $In_{0.4}Ga_{0.6}As_{0.995}N_{0.005}$ QW active region with $GaAs_{0.97}N_{0.03}$ barriers.

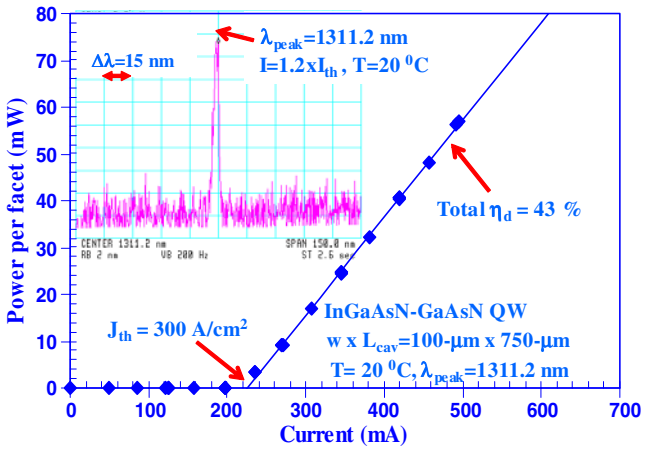

Figure 19. The relation of the output power per facet (P) and the total injected current (I) for $In_{0.4}Ga_{0.6}As_{0.995}N_{0.005}$ QW lasers with $GaAs_{0.97}N_{0.03}$ barriers ($L_{cav} = 1500\ \mu$m) at a temperature of 20 °C. The inset shows the lasing spectrum at 20 °C.

obtained for devices with a cavity length of 750 μm. The internal loss and the above-threshold current injection efficiency of the InGaAsN–GaAsN QW lasers are measured as approximately 9 cm^{-1} and 70%, respectively.

The gain characteristics (g) of the InGaAsN QW lasers in these studies are assumed to follow the conventional semi-logarithmic relation of $g_{th} = g_{0J} \ln(\eta_{inj} J_{th}/J_{tr})$, with g_{0J} defined as the material gain parameter. From measurements on devices with various cavity lengths, the material gain parameter (g_{0J}) and the transparency current density (J_{tr}) have been determined as approximately 1320 ± 50 cm^{-1} and 75 ± 5 A cm^{-2}. The measured g_{0J} and J_{tr} of the InGaAsN–GaAsN QW lasers reported here are comparable to those of InGaAsN QW lasers with GaAs barriers ($g_{0J} \sim 1150$–1200 cm^{-1} and $J_{tr} \sim 75$–80 A cm^{-2}) [9]. We find that the

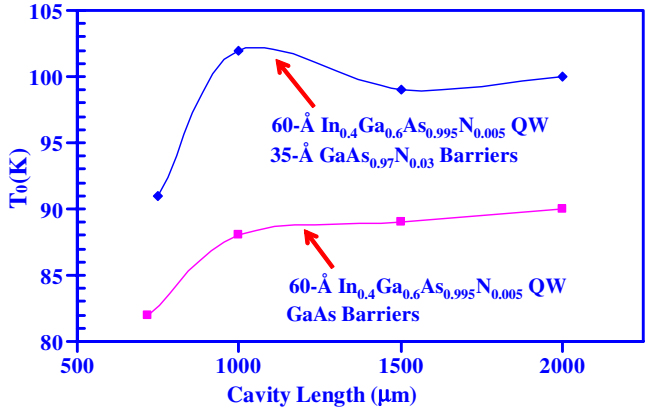

Figure 20. The comparison of the T_0 values measured for temperatures of 10–50 °C for $In_{0.4}Ga_{0.6}As_{0.995}N_{0.005}$ QW lasers with $GaAs_{0.97}N_{0.03}$ barriers and GaAs barriers, for various cavity lengths.

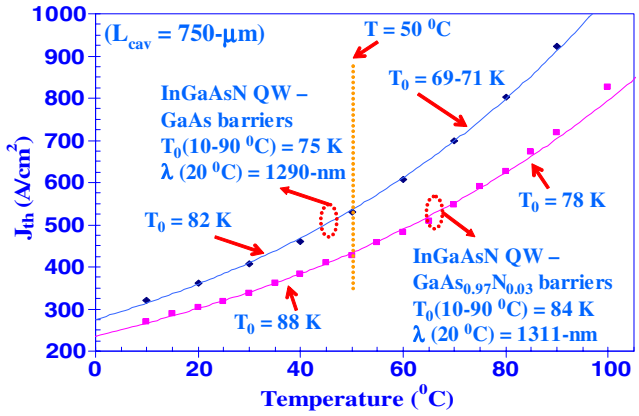

Figure 21. Threshold current densities (J_{th}) of $In_{0.4}Ga_{0.6}As_{0.995}N_{0.005}$–$GaAs_{0.97}N_{0.03}$ QW and $In_{0.4}Ga_{0.6}As_{0.995}N_{0.005}$–GaAs QW laser devices with the cavity length of 1000 μm, as functions of temperature in the range of 10–90 °C.

choice of the barrier material surrounding the InGaAsN QW is very important, significantly affecting the threshold characteristics of the lasers at elevated temperatures.

The characteristics of the InGaAsN–GaAsN QW lasers are measured for temperatures of 10–100 °C, with temperature steps of 5 °C. In the temperature range from 10 to 50 °C, the measured T_0 values ($1/T_0 = (1/J_{th})\,\mathrm{d}J_{th}/\mathrm{d}T$) of these lasers are as high as 100 K for devices with cavity lengths of 1000 and 2000 μm, as shown in figure 20. From our measurements on devices with various cavity lengths, the threshold characteristics of these 1311–1317 nm InGaAsN–GaAsN QW lasers is less temperature sensitive than the 1290–1295 nm InGaAsN QW lasers with GaAs barriers [9]. The increase in T_0 values for the InGaAsN–GaAsN QW lasers, in comparison to those for InGaAsN–GaAs QW lasers, is not accompanied by any increase in threshold current, as shown in figure 21. Very low threshold current densities of only 550 (and 520) A cm^{-2} and 715 (and 670) A cm^{-2} are also achieved for InGaAsN–GaAsN QW lasers with cavity lengths of 1500 and 750 μm, respectively, at temperatures of 90 (and 85) °C. The lasing wavelength shift with temperature is found to be a linear function

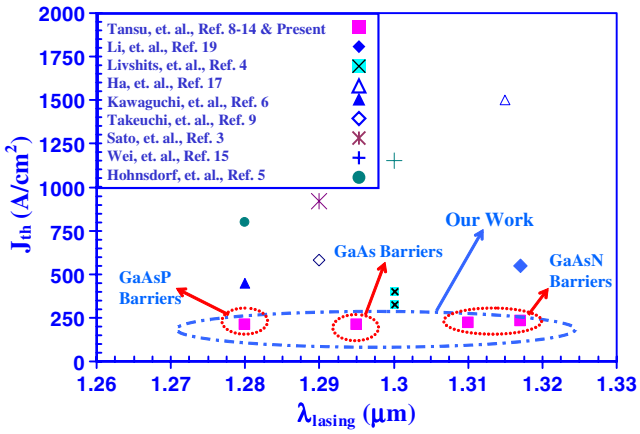

Figure 22. Comparison of threshold current densities of InGaAsN QW lasers in the wavelength region of 1260–1330 nm.

with a rate ($d\lambda/dT$) of approximately 0.39 nm K^{-1}, resulting in emission wavelengths beyond 1340–1345 nm for devices with a cavity length of 1500 μm at a temperature of 90 °C.

In earlier works [17–19], aside from strain compensation, the motivation for using GaAsN barriers surrounding the InGaAsN QW is to reduce the quantum confinement effect, which in turn results in a red-shift of the emission from the QW. We demonstrate here that, in addition to the wavelength red-shift, the utilization of GaAsN barriers surrounding the InGaAsN QW may also improve hole confinement in the QW, as is evident from the improved temperature performance. A slight type-II alignment of the GaAsN material system with the GaAs material system has been previously reported, with a very small negative valence band offset (ΔE_v) of 15–20 meV/%N [39–41], which would lead to a slight increase in the heavy hole confinement (ΔE_v) in InGaAsN QWs, as shown schematically in figure 18.

To place the results reported here in perspective, we plot the best reported threshold current densities for various InGaAsN QW lasers [4, 6–19] in figure 22. The previously lowest reported threshold current density of 546 A cm^{-2} for InGaAsN QW lasers with a cavity length of 1600 μm at an emission wavelength of 1317 nm was realized by the group at Tampere University of Technology utilizing MBE technology [18, 19]. To the best of our knowledge, the MOCVD-grown InGaAsN–GaAsN QW lasers reported here show the lowest threshold current densities for wavelengths beyond 1300 nm. Note that the threshold current density plots (in figure 22) for our various InGaAsN QW lasers are obtained from devices with cavity lengths of 1000–2000 μm, which exhibit slightly lower values in comparison to the shorter cavity devices (shown in figure 21, for $L_{cav} = 750$ μm).

In summary, we have realized $In_{0.4}Ga_{0.6}As_{0.995}N_{0.005}$ QW lasers employing $GaAs_{0.97}N_{0.03}$ barriers, with room temperature emission wavelengths of 1311–1317 nm. Threshold current densities of approximately 300, 270, 230, and 210 A cm^{-2} are measured for these devices for cavity lengths of 750, 1000, 1500, and 2000 μm, respectively. Merely changing the barrier material from GaAs to GaAsN, we find improved device temperature characteristics in addition to a red-shift in the emission wavelength. This improvement may be accounted for by the improved heavy hole confinement in the GaAsN barrier structures. The weak dependence of the threshold current densities on emission wavelength for the range of 1280–1317 nm also indicates potential for high performance InGaAsN QW lasers with emission wavelengths even beyond 1320 nm.

8. Comparison of MOCVD-grown InGaAsN with other InGaAsN samples in the 1300 nm regions

In the last few years, there has been significant progress in the development of MOCVD-grown 1300 nm InGaAsN QW lasers. The achievement in the MOCVD-grown InGaAsN QW lasers is of extreme importance, due to its significance for realizing manufacturable InGaAsN QW VCSEL devices. The MOCVD growth technology is more compatible with realizing VCSEL devices, because of its higher growth rates. MOCVD technology also offers better compositional grading and doping control in the heterointerfaces, which are essential for realizing low resistivity DBR layers.

We make in table 1 threshold current density comparisons for various InGaAsN QW lasers. The results presented here represent the best results for InGaAsN QW lasers in the wavelength region around 1300 nm. Our results for 1300 nm InGaAsN QW lasers are for strain-compensated $In_{0.4}Ga_{0.6}As_{0.995}N_{0.005}$ QW active materials. Our 1300 nm InGaAsN QW lasers are realized with transparency and threshold current densities of approximately 75–85 and 200–250 A cm^{-2}, respectively.

The transparency and threshold current densities of the 1300 nm InGaAsN QW lasers that we realized here still represent the lowest transparency current densities ever reported for this wavelength region. The best reported lasing performances for MBE-grown InGaAsN QW lasers were realized by Livshits *et al* [4] of Infineon Technologies (Germany) and Peng *et al* [18] of Tampere University of Technology. It is important to note that our results reported here still represent the only ones for high performance 1300 nm InGaAsN QW lasers grown using conventional technology with AsH_3 as the As precursor. Other MOCVD investigations achieving high performance, realized by Takeuchi *et al* [26] of Agilent Technologies Laboratories (USA) and Kawaguchi *et al* [6] of the Tokyo Institute of Technology (Japan), utilized TBA as the As precursor.

9. Single-mode ridge waveguide 1300 nm InGaAsN QW lasers

Over the past few years, improved single-mode InGaAsN ridge waveguide laser performance has been realized by both MOCVD and MBE [42–46]. Illek and co-workers [42] demonstrated MBE-grown lasers emitting at 1.28 μm with a threshold current of 11 mA under pulsed operation and a high reflectivity coated facet (HR/as-cleaved). For MOCVD-grown InGaAsN ridge waveguide lasers, 1.295 μm emitting double-QW devices with threshold currents of 75 mA under pulsed operation were reported by Sato and Satoh [45]. By utilizing the strain-compensation technique for GaAsP barriers [9], we successfully achieved high performance MOCVD-grown single-mode InGaAsN QW as-cleaved ridge waveguide lasers at 1.292 μm. The CW threshold current around 15 mA at room temperature is currently the best result reported for the MOCVD growth technique and is comparable to the best MBE result.

The laser structure and growth conditions here are similar to those described in sections 2–4 as shown in figures 1 and 23. The structure consists of a 6 nm $In_{0.4}Ga_{0.6}As_{0.995}N_{0.005}$ QW obtained with a growth temperature of 530 °C, with its composition calibrated by secondary-ion mass spectroscopy measurement. The growth rate of the QW is approximately 1.28 μm h^{-1}. On both sides of the InGaAsN QW, 75 Å $GaAs_{0.85}P_{0.15}$ tensile strain layers were employed for strain compensation with 100 Å GaAs setback layers. The SCH consists of 300 nm undoped GaAs, with both n- and p-type cladding layers consisting of 1.1 and 0.9 μm thick $Al_{0.75}Ga_{0.25}As$ layers, respectively. The width and height of the ridge structure are 4 and 1 μm, respectively; it was formed by standard photolithography techniques and chemical wet etching with $NH_4OH:H_2O_2:H_2O = 3:1:50$ solution. The lateral effective index step is calculated to be

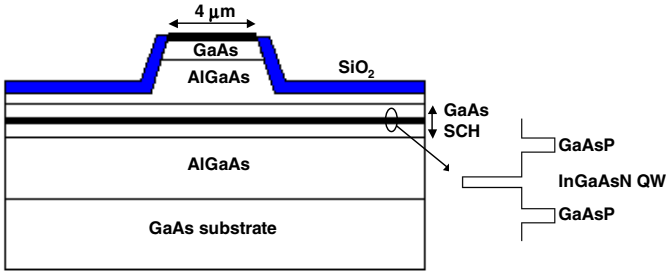

Figure 23. The schematic device structure of the InGaAsN–GaAs ridge waveguide lasers.

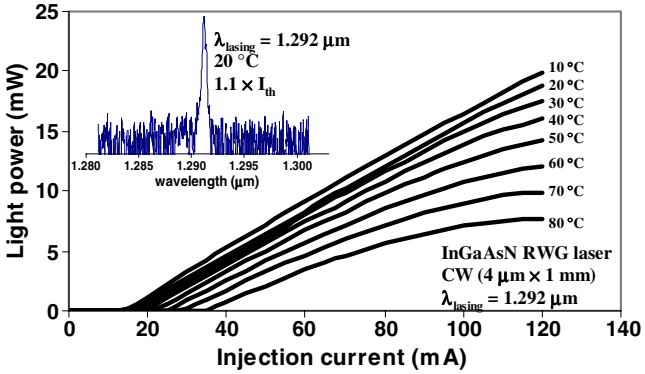

Figure 24. Continuous wave light–current characteristics of 4 μm $\times$ 1 mm single-QW InGaAsN ridge waveguide lasers at various heat sink temperatures. Inset: the lasing spectrum at 20 °C for 1 mm long as-cleaved devices. The peak wavelength is at 1.292 μm.

0.023 using the effective index approximation and the transition matrix method. A 1000 Å thick SiO_2 layer was deposited by plasma enhanced chemical vapour deposition (PECVD) for current confinement and surface passivation. Alloys of Ti/Pt/Au and Ge/Ni/Au, as p- and n-type contact layers, were deposited by electron beam evaporator and rapidly annealed at 370 °C for 30 s under forming gas. The device schematic structure is shown in figure 23. The cleaved devices were mounted p side up on copper heat sinks without facet coating for the light–current (P–I) and far field measurements under CW conditions.

Figure 24 shows the CW P–I curves for 1 mm long InGaAsN ridge waveguide lasers over a temperature range from 10 to 80 °C. The threshold current is only 15.5 mA at 20 °C, corresponding to a threshold current density of 388 A cm^{-2}. This represents the lowest value reported for InGaAsN ridge waveguide lasers emitting at 1.3 μm, and is comparable with that for conventional InGaAsP–InP QW lasers, showing the promise for this material system [47–49]. The higher threshold current density compared to that of broad area devices (253 A cm^{-2}) with identical structure is possibly due to lateral current spreading. With a shorter cavity length of 800 μm, the threshold current is only 14 mA. The maximum output power per facet is 24 mW at 20 °C and this reduces to 8 mW at 80 °C, limited by device heating. The turn-on voltage and device resistance were measured to be 1.15 V and 12 Ω respectively. The relatively large series resistance (possibly a result of the high Al content cladding layers) results in strong Joule heating in the junction and degrades the laser maximum CW output power. The lasing spectrum is shown in figure 24 and the peak wavelength is 1.292 μm at 20 °C. At 80 °C, the lasing wavelength shifts to 1.32 μm with a wavelength temperature dependence $\lambda_{\text{lasing}}(T)$ of 0.5 nm °C^{-1}.

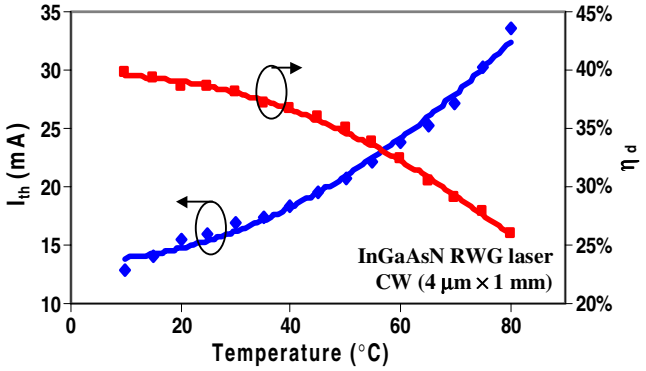

Figure 25. The temperature dependence of the threshold current and external differential quantum efficiency. The characteristic temperatures T_0 and T_1 are 93 and 227 K (20–60 °C), respectively.

The InGaAsN ridge waveguide laser threshold current (I_{th}) and external differential quantum efficiency (η_d) characteristics as a function of the heat sink temperature are shown in figure 25, for 1 mm long devices, from 10 to 80 °C. At 60 °C, the threshold current increases to 23.8 mA and the measured T_0 is 93 K (20–60 °C). Comparing η_d at 20 and 60 °C, we see that it decreases from 39% to 32% and the T_1 value is 227 K. The temperature dependence of the InGaAsN laser characteristics shows inferior performance compared to the 1.23 μm emitting InGaAs ridge waveguide laser with an identical device structure, where T_0 and T_1 values of 143 and 357 K were obtained. Nevertheless, a T_0 value of 93 K is significantly greater than the typical value of 50 K for conventional 1.3 μm emitting InGaAsP–InP ridge waveguide lasers [47, 48, 9] and quite comparable to that for AlGaInAs–InP QW lasers [50, 51].

At a heat sink temperature of 25 °C, the far field patterns (FFP) of the laser beam in the lateral direction have a full width at half-maximum (FWHM) of 20.7° for $I = 20$ mA and 22.2° for $I = 80$ mA. The field pattern indicates single-mode operation for these ridge waveguide devices at low output power levels. At higher drive currents, multi-mode operation or beam instabilities occur. Utilization of a smaller ridge width (<3 μm) is expected to stabilize the optical mode to higher output powers.

In these experiments, low threshold single-mode InGaAsN single-QW as-cleaved ridge waveguide lasers were achieved by MOCVD. The threshold current is only 15.5 mA under continuous wave operation for as-cleaved devices with 4 μm ridge width and 1 mm cavity length. For 800 μm long ridge waveguide lasers, the threshold current is only 14 mA. The lasing wavelength is 1.292 μm with a maximum output power of 24 mW at 20 °C. T_0 and T_1 values of 93 and 227 K were obtained and indicate improved high temperature characteristics compared to conventional InP-based ridge waveguide lasers. The lateral far field pattern indicates single-mode operation near the laser threshold.

10. Extension of InGaAsN QW lasers beyond 1320 nm

Recent promising results [1–19] have shown tremendous potential for InGaAsN QW lasers as an alternative material system for replacing the conventional InP technology in the wavelength region of 1300 nm, as shown also in earlier sections. InGaAsN QW lasers have demonstrated impressive results for devices with emission wavelengths around 1300 nm [1–19], as shown earlier in sections 3, 4 up to 9. Few results on InGaAsN QW lasers with emission wavelength around 1370–1400 nm have been published with reasonable lasing

performance [5, 15, 17, 52, 53]. Threshold current densities of approximately 1.85–2.5 kA cm^{-2} [5, 15, 17, 52, 53] have been reported for InGaAsN QW lasers, grown by MBE and MOCVD, in the wavelength region of 1370–1400 nm. Several MOCVD-grown InGaAsN QW lasers have been demonstrated with threshold current densities of 2.5 and 2.2 kA cm^{-2} for emission wavelengths of 1370 nm [52] and 1380 nm [5], respectively. Recent efforts, utilizing chemical beam epitaxy, have also resulted in 1400 nm InGaAsN QW lasers with threshold current densities of approximately 8.9 kA cm^{-2} [54]. Realization of low threshold current density and temperature insensitive 1400 nm diode lasers is essential for high performance and low cost pump lasers for Raman amplifiers.

Here we report on high performance InGaAsN QW lasers on GaAs with emission wavelengths ranging from 1360 to 1382 nm, obtained by utilizing low pressure MOCVD. The design of the active region utilizes a highly compressive, very high In content (40%), InGaAsN QW, with a minimal N content of approximately 1%, to achieve emission wavelengths of 1360 nm and 1382 nm. Tensile-strained barriers of GaAsP are utilized to partially strain compensate the QW active region.

The laser structures studied here, as shown in figure 1, consist of a 60 Å ($\Delta a/a = 2.7\%$) $In_{0.4}Ga_{0.6}AsN$ single-QW active layer with GaAs layers bounding the QW. Partial strain compensation of the highly strained InGaAsN QW is achieved by utilizing $GaAs_{0.85}P_{0.15}$ tensile-strained layers offset from the QW [8, 9], and a tensile-strained buffer layer of $GaAs_{0.67}P_{0.33}$ [9] as shown in figure 1. The benefit and purpose of the various strain compensating layers have been demonstrated and elaborated on in our earlier studies discussed in sections 2–4. The lower and top cladding layers of the lasers consist of 1.1 μm thick $Al_{0.74}Ga_{0.26}As$ layers with doping levels of 1×10^{18} cm^{-3} for both the n and p cladding layers, respectively. The growth temperatures of the n- and p-$Al_{0.74}Ga_{0.26}As$ are 775 and 640 °C, respectively. The annealing of the InGaAsN QW is accomplished during the growth of the top cladding layer at a temperature of 640 °C, with a duration of approximately 27 min.

From our prior work described in section 2, we found that a DMHy/V ratio of 0.961 is required to realize 60 Å $In_{0.4}Ga_{0.6}As_{0.995}N_{0.005}$–GaAs QW active regions with an emission wavelength of 1300 nm. The extension of the emission wavelength of the InGaAsN QW laser is achieved by increasing the N content in the InGaAsN QW, while maintaining the In content and the QW thickness constant at 40% and 60 Å, respectively. The incorporation of N in the InGaAs material system is a very strong function of the DMHy/V ratio. By increasing the DMHy/V ratio, larger N content InGaAsN QW can be realized. Utilizing DMHy/V ratios of 0.975 and 0.980, the lasing emission wavelengths of the 60 Å $In_{0.4}Ga_{0.6}AsN$ QW active regions are extended up to 1360 and 1382 nm, respectively. The N contents in the 1360 and 1382 nm InGaAsN QWs are estimated as approximately 0.8% and 0.85%, respectively, as calibrated from the growth conditions.

Broad area lasers, with a stripe width (w) of 100 μm, were fabricated utilizing the InGaAsN QW active regions for emission wavelengths at 1360 and 1380 nm. The lasing characteristics are measured under pulsed currents with a pulse width of 5 μs and duty cycle of 1%. The measurements were performed on as-cleaved broad area laser devices, with an oxide-defined stripe width of 100 μm. The metal contacts were realized with 250 Å Ti/500 Å Pt/1500 Å Au and 200 Å Ge/1000 Å GeAu/500 Å Ni/3000 Å Au for the p contact and n contact, respectively. The contact annealing of the devices was accomplished under forming gas (10% H_2 + 90% N_2) at a temperature of 370 °C for a duration of 30 s.

The pulsed lasing characteristics of the 1360 nm InGaAsN QW lasers with a cavity length (L_{cav}) of 1000 μm are shown in figure 26. A room temperature threshold current density (J_{th}) of only 520 A cm^{-2} is achieved for InGaAsN QW lasers with L_{cav} of 1000 μm, at an emission wavelength of 1357 nm. An external differential quantum efficiency of approximately 43.2%

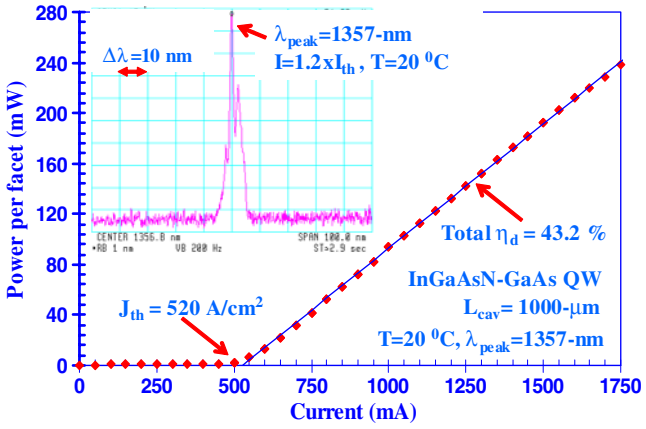

Figure 26. The measured output power versus current (P–I) characteristics of the 1360 nm InGaAsN QW lasers with $L_{\rm cav} = 1000$ μm, at a temperature of 20 °C. The inset shows the near threshold lasing spectrum at a heat sink temperature of 20 °C.

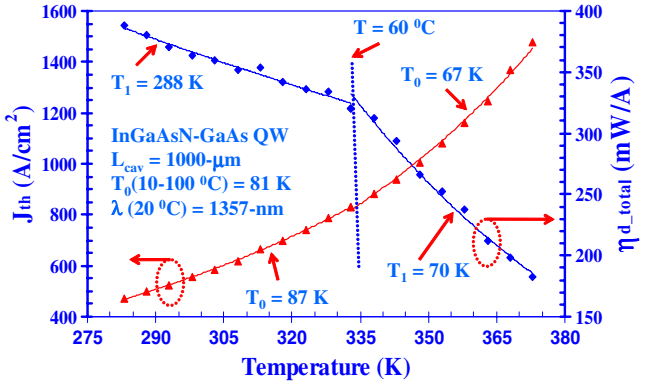

Figure 27. The measured $J_{\rm th}$ and $\eta_{\rm d}$ for 1360 nm InGaAsN QW lasers as a function of temperature.

is also measured. The threshold current density of longer cavity devices ($L_{cav} = 1500$ μm) is measured as only 450 A cm^{-2} at a temperature of 20 °C. Accompanying the large shift in the emission wavelength from 1300 to 1360 nm, the threshold current density of the 1360 nm InGaAsN QW is increased by approximately a factor of two [9].

The temperature dependence of the threshold current density of the 1360 nm InGaAsN QW lasers with a cavity length of 1000 μm is shown in figure 27. The characteristic temperature coefficients of the threshold current density (T_0 values, with $1/T_0 = 1/J_{\rm th}[{\rm d}J_{\rm th}/{\rm d}T]$) of 87 and 67 K are measured in the temperature ranges of 10–60 °C and 60–100 °C, respectively. A threshold current density of 1480 A cm^{-2} is measured at a heat sink temperature of 100 °C, with an emission wavelength of approximately 1400 nm.

The dependence of the external differential quantum efficiency for the 1360 nm InGaAsN QW lasers as a function of temperature is shown in figure 27. At elevated temperatures, the slope efficiency of this laser is extremely temperature sensitive, as reflected by the low T_1 value ($1/T_1 = -1/\eta_{\rm d}[{\rm d}\eta_{\rm d}/{\rm d}T]$) of only 70 K for the temperature range of 60–100 °C. By comparison, optimized 1233 nm emitting $In_{0.4}Ga_{0.6}As$ QW lasers typically exhibit T_1 values of 1250 K [25].

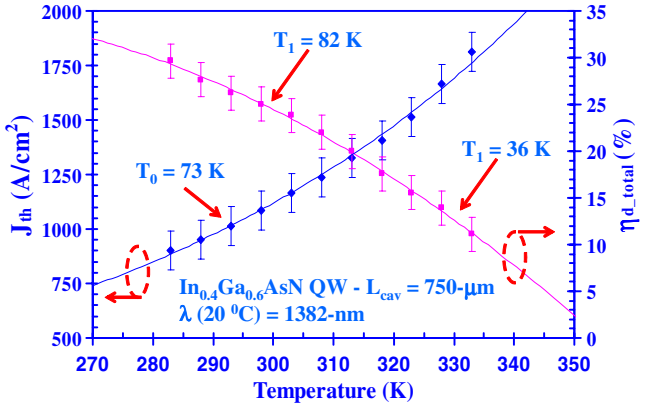

Figure 28. The measured J_{th} and η_d for 1382 nm InGaAsN QW lasers as a function of temperature.

The pulsed lasing characteristics of the 1382 nm InGaAsN QW lasers are shown in figure 28, for a device with a cavity length of 750 μm. By increasing the DMHy/V ratio to 0.980, emission wavelengths up to 1382 nm were realized for laser devices with a cavity length of 750 μm at a heat sink temperature of 20 °C. Threshold current densities of approximately 900, 1010, and 1800 A cm^{-2} were achieved for InGaAsN QW lasers at heat sink temperatures of 10, 20, and 60 °C, respectively.

One of the interesting characteristics of the 1382 nm InGaAsN QW lasers is the fact that the external differential quantum efficiency exhibits a very strong temperature sensitivity. The T_1 value of the 1382 nm InGaAsN QW lasers is only 82 K in the temperature range of 10–40 °C, which is extremely low in comparison to that ($T_1 = 360$ K for the temperature range of 10–60 °C [9]) of the 1300 nm InGaAsN QW lasers. As we increase the N content in the InGaAsN QW to extend the emission wavelength, severe carrier leakage from the QW may occur as a result of a significant reduction in the hole confinement for larger N content InGaAsN QWs [38].

Even though the threshold current densities of the MOCVD-grown 1360 and 1382 nm InGaAsN QW lasers reported here are higher than for the lower N content 1300 nm InGaAsN QW lasers, these results still represent the best reported threshold current densities in the wavelength region of 1360–1400 nm, as shown in figure 29. In figure 29, we have plotted the best reported threshold current densities of InGaAsN QW lasers for the wavelength range from 1360 to 1400 nm [5, 14, 15, 17, 52, 53]. Some of the best reported J_{th} values for MOCVD-grown InGaAsN QW lasers with emission wavelengths of 1370 and 1380 nm were realized by Agilent Technologies Laboratories [52] and Philip University of Marburg [53], respectively, with threshold current densities in the range of 2200–2500 A cm^{-2}. The results from Agilent Technologies Laboratories and Philip University of Marburg both utilize TBA as the As precursor. The MOCVD-grown InGaAsN QW lasers reported here exhibit record-low threshold current densities (at $T = 20$ °C) of only 450–520 A cm^{-2} and 1010 A cm^{-2} for emission wavelengths at 1360 and 1382 nm, respectively. These efforts demonstrate that high performance 1360 and 1382 nm InGaAsN QW lasers can be realized with AsH_3 as the As precursor.

In figure 30, we give a summary of the best reported InGaAs QW and InGaAsN QW lasers on GaAs from the emission wavelength of 1100 up to 1400 nm. As shown in figure 30, we recently realized InGaAsN QW lasers with a threshold current density of only approximately

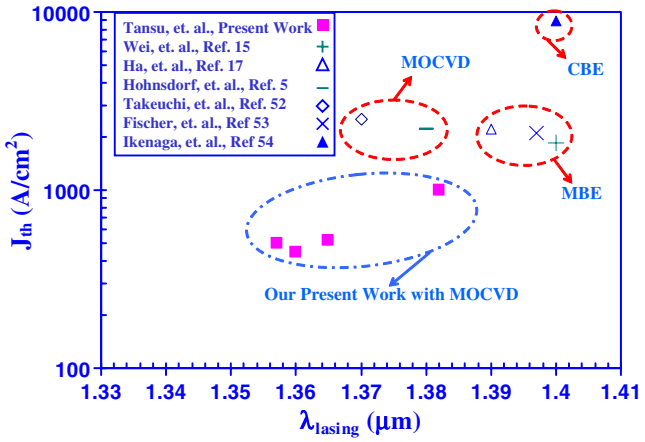

Figure 29. Comparison of the threshold current densities for various InGaAsN QW lasers with emission wavelengths of 1350–1410 nm.

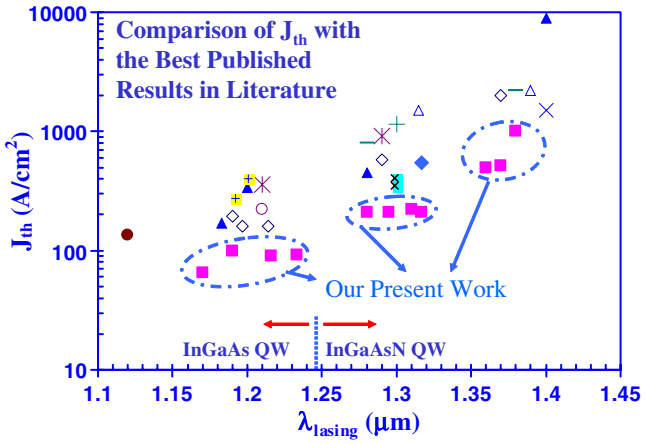

Figure 30. Comparison of threshold current densities for various InGaAs(N) QW lasers with emission wavelengths from 1170 nm up to 1400 nm.

500 A cm^{-2} for emission wavelengths up to 1370 nm. Our reported J_{th} value for 1370 nm InGaAsN QW lasers is extremely low in comparison to some of the published results for InGaAsN QWs at wavelengths of 1370–1400 nm. The fact that low J_{th} InGaAsN QW lasers have been realized with MOCVD technology indicates the large potential for pushing this material system to applications beyond 1400–1550 nm. One of the main challenges in pushing the MOCVD-grown InGaAsN QW system is the difficulty in incorporating more N into the high In content InGaAs—to push the emission wavelength beyond 1400–1550 nm.

11. Temperature analysis of the InGaAsN QW lasers

Recent temperature analyses of InGaAsN diode lasers in the 1300 nm wavelength region indicate that Auger recombination [28] and hole leakage [29, 30, 38] may play a significant role in the observed temperature sensitivity of the threshold current density and external

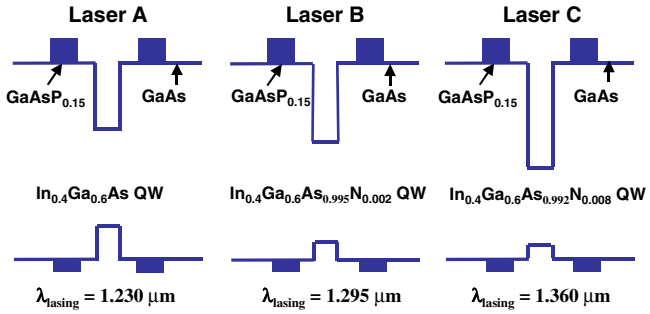

Figure 31. A schematic band diagram of the InGaAs(N) QW laser structures with N contents of 0%, 0.5%, and 0.8% for 1230 nm $In_{0.4}Ga_{0.6}As$ (laser A), 1295 nm $In_{0.4}Ga_{0.6}As_{0.995}N_{0.005}$ (laser B), and 1360 nm $In_{0.4}Ga_{0.6}As_{0.992}N_{0.008}$ (laser C) QW lasers, respectively.

differential quantum efficiency. To achieve emission wavelengths beyond 1300 nm, higher N content InGaAsN active regions have been obtained by various growth techniques such as MBE [6, 15, 17], MOCVD (see [6, 52] and our work in section 10), and chemical beam epitaxy (CBE) [54]. With much higher threshold current density and lower external differential quantum efficiency than for 1300 nm emitting lasers, these devices also showed severe temperature sensitivity of the laser characteristics. However, no study has yet focused on the strong temperature dependence of InGaAsN QW lasers beyond 1300 nm and the underlying mechanism is still uncertain.

In this work, we present a temperature analysis of InGaAs(N) QW lasers over a wide emission wavelength range from 1230 to 1360 nm obtained by simply adjusting the nitrogen composition in the QW. It was found that incorporation of higher nitrogen content significantly degraded the laser characteristics *and* temperature performance. Furthermore, we conclude that this behaviour can be attributed to the highly temperature sensitive current injection efficiency and material gain parameter for InGaAsN QW lasers with higher N content.

The InGaAs QW and InGaAsN QW laser structures were similar to the ones studied earlier, as shown in figure 1. In this study, we focused on three MOCVD-grown InGaAs(N) QW lasers with lasing wavelengths of 1.230 μm (laser A) [25], 1.295 μm (laser B) [9], and 1.360 μm (laser C) (see section 10) for 2 mm long devices, respectively; the schematic band diagrams are shown in figure 31. A high In content of 40% was utilized in the QW grown at a temperature of 530 °C for all three laser bases. The only distinction between these laser structures was the nitrogen composition x of the 60 Å thick $In_{0.4}Ga_{0.6}As_{1-x}N_x$ QW, which was determined as 0% and 0.5% for lasers A and B, calibrated by secondary-ion mass spectroscopy measurements, and 0.8% for laser C, estimated by extrapolating the growth parameters. The calculated strains of the InGaAs(N) QWs are −2.79%, −2.69%, and −2.64% for lasers A–C, respectively. The minimum strain variation of the active regions utilized here should not result in any significant difference in laser characteristics contributed from the strain difference. The detailed laser structure has been described in the earlier sections. The optical confinement factor (Γ) of 1.7% was calculated for all three structures by using the transmission matrix method.

As-cleaved broad area lasers were fabricated with a stripe width of 100 μm and the lasing characterization was conducted at a heat sink temperature range from 10 to 100 °C with a pulse width of 5 μs (1% duty cycle). No heating was observed during the optical power versus injection current measurement under the experimental conditions. The threshold current density (J_{th}) was 110, 266, and 513 A cm^{-2} and the external differential quantum

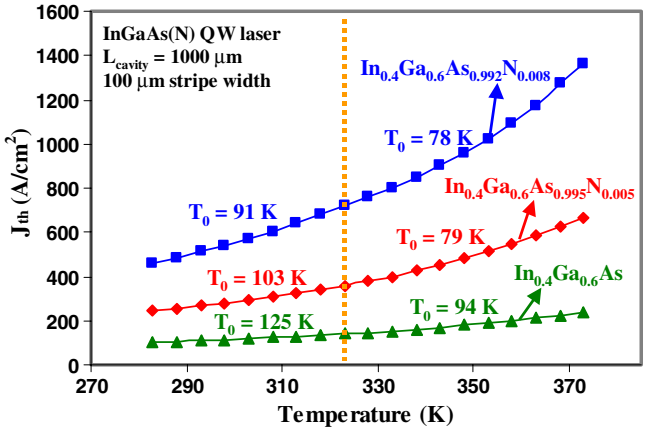

Figure 32. $J_{\rm th}$ as a function of temperature for lasers A–C with 1000 μm cavity length.

efficiency ($\eta_{\rm d}$) was 48%, 46%, and 43% at 20 °C for the 1 mm cavity length devices of lasers A, B, and C, respectively. Figures 32 and 33 show the detailed temperature dependence of $J_{\rm th}$ and $\eta_{\rm d}$ as well as the characteristic temperatures T_0 and T_1 ($1/T_0 = 1/J_{\rm th}({\rm d}J_{\rm th}/{\rm d}T)$ and $1/T_1 = -1/\eta_{\rm d}({\rm d}\eta_{\rm d}/{\rm d}T)$) for temperature ranges of 10–50 °C and 50–100 °C. These data indicate that the 1230 nm $In_{0.4}Ga_{0.6}As$ QW lasers (laser A) have both the lowest $J_{\rm th}$ and the largest $\eta_{\rm d}$ as well as higher T_0 and T_1 values compared with the 1295 nm $In_{0.4}Ga_{0.6}As_{0.995}N_{0.005}$ (laser B) and 1360 nm $In_{0.4}Ga_{0.6}As_{0.992}N_{0.008}$ (laser C) QW lasers. The T_0 values from 20 to 60 °C were characterized as 120, 98, and 88 K and the T_1 values are 631, 333, and 227 K for lasers A–C, respectively, indicating a trend of reduction in T_0 and T_1 for the lasers with higher N contents in the QWs. At 100 °C, the InGaAs QW lasers exhibited a very low $J_{\rm th}$ of 237 A cm^{-2} and a high $\eta_{\rm d}$ of 41%. It is concluded that with increasing N content in the InGaAsN QW, the lasers show degraded lasing characteristics and, more importantly, significantly higher temperature sensitivity, although an extension of the lasing wavelength can be achieved.

It has been shown that the characteristic temperatures T_0 and T_1 can be expressed by equations (1) and (2), assuming that $J_{\rm th}$, the transparent current density ($J_{\rm tr}$), and the internal loss ($\alpha_{\rm i}$) increase exponentially with temperature while $\eta_{\rm d}$, the current injection efficiency ($\eta_{\rm inj}$), and the material gain parameter (g_{0J}) decrease exponentially. The relations can be written as [24, 29]

$$\frac{1}{T_0(L)} = \frac{1}{T_{\rm tr}} + \frac{1}{T_{\eta_{\rm inj}}} + \frac{\alpha_{\rm i} + \alpha_{\rm m}(L)}{\Gamma g_{0J}} \frac{1}{T g_{0J}} + \frac{\alpha_{\rm i}}{\Gamma g_{0J}} \frac{1}{T \alpha_{\rm i}}, \tag{1}$$

$$\frac{1}{T_1(L)} = \frac{1}{T_{\eta_{\rm inj}}} + \frac{\alpha_i}{\alpha_{\rm i} + \alpha_{\rm m}(L)} \frac{1}{T \alpha_i}, \tag{2}$$

where $T_{\rm tr}$, $T_{\eta_{\rm inj}}$, $T_{g_{0J}}$, and $T_{\alpha_{\rm i}}$ are the characteristic temperatures of $J_{\rm tr}$, $\eta_{\rm inj}$, g_{0J}, and $\alpha_{\rm i}$, and $\alpha_m(L) = (1/L)\ln(1/R)$ is the mirror loss as a function of the cavity length where R is the facet reflectivity and L is the cavity length. In order to discern the dominant mechanism for the poor temperature performance of the long wavelength 1360 nm InGaAsN QW lasers, temperature characteristics of $J_{\rm tr}$, $\eta_{\rm inj}$, and g_{0J} were obtained from a series of temperature dependent length studies. By deducing the slope and intercept of the $1/\eta_{\rm d}$ versus L data line, one can calculate the laser intrinsic parameters $\alpha_{\rm i}$ and $\eta_{\rm inj}$ on the basis of the following equation:

$$\eta_{\rm d} = \eta_{\rm inj} \frac{\alpha_{\rm m}(L)}{\alpha_{\rm i} + \alpha_{\rm m}(L)}. \tag{3}$$

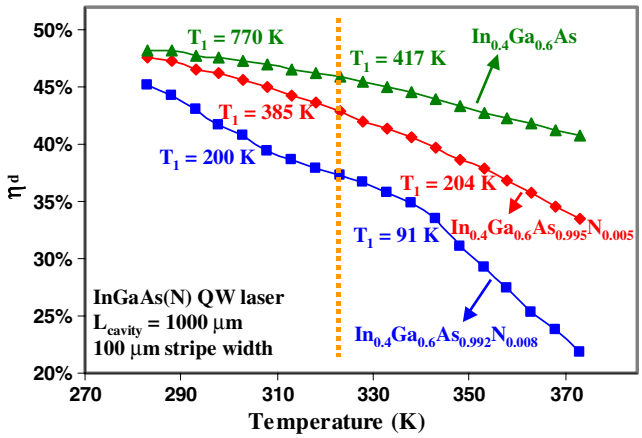

Figure 33. η_d as a function of temperature for lasers A–C with 1000 μm cavity length.

Also, from the logarithmic relation of the threshold gain (g_{th}) and threshold current density shown as equation (4), g_{0J} and J_{tr} can be extracted:

$$g_{th} = g_{0J} \ln\left(\frac{\eta_{inj} J_{th}}{J_{tr}}\right). \tag{4}$$

The result of length studies for these three laser structures is shown in figure 34, where η_{inj} is expressed as a function of the heat sink temperature from 10 to 100 °C. Current injection efficiency (η_{inj}) values of 81%, 66%, and 53% at room temperature and $T_{\eta_{inj}}$ values of 2000, 354, and 161 K were observed for the InGaAs(N) QW lasers with 0%, 0.5%, and 0.8% N contents, respectively. The strong temperature dependence of the injection efficiency indicates a much stronger carrier leakage process for the high N content InGaAsN QW lasers. At 100 °C, η_{inj} for laser C reduces to 31% while η_{inj} for laser A is still as high as 78%. The second term in equation (2) represents the contribution from the internal loss temperature sensitivity. Values of $T_{\alpha_i} \times (\alpha_i + \alpha_m)/\alpha_i$ were measured and calculated to be 640, 1153, and 2132 for lasers A–C, respectively, and the $T_{\alpha i}$ values are 260, 360, and 400 K. According to equation (2), we can determine that the factor which limits T_1 for the InGaAs QW laser is the internal loss (the second term) since $T_{\eta inj}$ hardly affects T_1 due to its large value of 2000 K. In contrast, the dominant factor resulting in the highly temperature sensitive η_d (a much lower T_1) for the 1295 and 1360 nm InGaAsN QW lasers is the current injection efficiency $\eta_{inj}(T)$ (the first term). The observed poor η_{inj} and $T_{\eta inj}$ values could presumably be explained by a hole leakage mechanism in InGaAsN QW lasers [11, 29, 38] with a reducing valence band offset as the nitrogen composition increases [55].

Unlike in equation (2) where $T_{\eta inj}$ is the dominant factor, the more complicated dependence of equation (1) leads to difficulty in analysing the dominant mechanism responsible for the degraded T_0 of InGaAsN QW lasers with increasing N content. For the analysis of T_0, the first three terms in equation (1) are considered important and need to be carefully examined. In figure 35, the measured g_{0J} values versus temperature are shown over the range 10–100 °C. The g_{0J} values at room temperature are measured to be 1800, 1432, and 1330 cm^{-1} and the $T_{g_{0J}}$ values are 620, 456, and 192 K for lasers A–C, respectively. The 1360 nm InGaAsN QW lasers exhibit inferior gain characteristics compared with the other two structures and with such a low $T_{g_{0J}}$, the g_{0J} value drops rapidly as temperature elevates and reaches a very low value of 800 cm^{-1} at 100 °C. Possible mechanisms accounting for this behaviour are non-radiative Auger recombination, nitrogen-induced change of the band structure, and

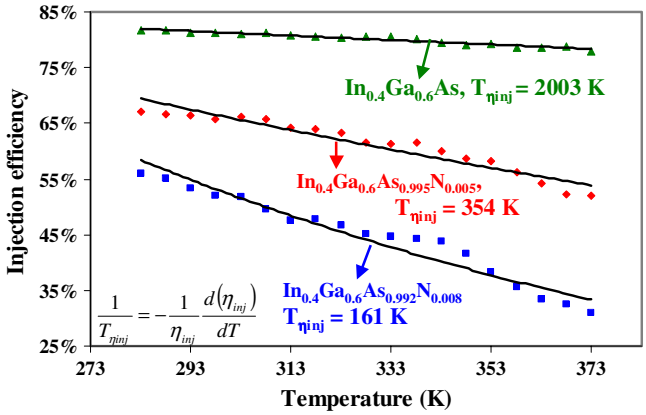

Figure 34. The relation between the current injection efficiency $\eta_{\rm inj}$ and temperature for the three laser structures. A higher $T_{\eta_{\rm inj}}$ was observed for the structure with less nitrogen in the QW.

a temperature sensitive carrier leakage process below threshold for lasers with higher N content. To improve our understanding, g_{0J} and $T_{g_{0J}}$ for $In_{0.35}Ga_{0.65}As_{0.992}N_{0.008}$ QW lasers are compared with those for $In_{0.4}Ga_{0.6}As_{0.995}N_{0.005}$ QW lasers, whose lasing wavelengths are designed to be 1.3 μm for both cases. With identical band-gap energy, the contributions from Auger recombination are considered to be similar for these two laser structures. However, the results of a lower g_{0J} of 1251 cm^{-1} (at 20 °C) and $T_{g_{0J}}$ of 330 K (from 10 to 60 °C) for $In_{0.35}Ga_{0.65}As_{0.992}N_{0.008}$ QW lasers indicate that mechanisms *other* than Auger recombination are also crucial for explaining the degradation of g_{0J} and $T_{g_{0J}}$. From these data, it can be concluded that increasing the N content in InGaAsN QW not only significantly reduces $\eta_{\rm inj}$ and $T_{\eta{\rm inj}}$, but also seriously degrades g_{0J} and $T_{g_{0J}}$. On the basis of this study, it is believed that the observed lowering T_0 and T_1 for InGaAsN QW lasers with increasing N content can be explained by the combination of a more severe carrier leakage process and stronger temperature dependence of g_{0J} [29, 30].

In this section, the studies demonstrate that the N content in the InGaAsN QW dramatically affects the temperature sensitivity of $\eta_{\rm inj}$ and g_{0J}. The strong temperature dependence of $\eta_{\rm inj}$ and g_{0J} leads to low values of T_0 and T_1 for the InGaAsN QW lasers with higher N content. The current injection efficiency of InGaAsN QW lasers exhibits increasing temperature sensitivity with increasing N content, which could result from a reduction of the heavy hole confinement. In the following sections, theoretical calculations and careful experiments demonstrate that suppression of thermionic heavy hole escape from the InGaAsN QW systems leads to significantly improved lasing performances at high temperature.

12. The thermionic emission lifetime of InGaAsN QW lasers

As presented in the studies in section 11, the stronger temperature sensitivity of the current injection efficiency of InGaAsN QW lasers with increasing N content leads to InGaAsN QW lasers with lower T_0 and T_1 values. In our earlier work [19, 30], the reduced T_0 and T_1 ($1/T_1 = -(1/\eta_{\rm d})\,{\rm d}\eta_{\rm d}/{\rm d}T$, $\eta_{\rm d}$ = external differential quantum efficiency) values of the 1300 nm InGaAsN QW lasers, compared to 1190 nm InGaAs QW lasers, has been linked primarily to an increase in the carrier/current leakage processes. Despite the deeper QW structure in the InGaAsN QW lasers, the *experimentally measured* current injection efficiency

($\eta_{\rm inj}$) of the 1300 nm InGaAsN QW reduces more rapidly with temperature compared to that of the 1200 nm InGaAs QW lasers [19]. As N is added into the QW to push the emission wavelength longer, experiments have indicated that the $\eta_{\rm inj}$ of InGaAsN QW lasers decreases as a function of increasing N content [8, 15]. The reduction in $\eta_{\rm inj}$ can result in active layer carrier leakage. Here we identify a carrier leakage process in InGaAsN QW lasers [19] as heavy hole leakage due to poor active layer hole confinement.

The thermionic carrier lifetime ($\tau_{\rm e}$) in QW lasers is an important factor in determining the current injection efficiency ($\eta_{\rm inj}$) of a laser [56, 57]. A large thermionic lifetime of the carriers in the QW indicates a minimal rate of escape of the carriers from the QW to the separate confinement heterostructure (SCH) [56, 57]. A minimal rate of escape thermionic carriers out of the QW will lead to an increase in $\eta_{\rm inj}$ and a reduction in the temperature sensitivity of $\eta_{\rm inj}$ [56, 57]. The conventional method for expressing the thermionic lifetime is based on the model by Schneider *et al* [58], which utilizes the bulk (3D) density of states (DOS) and a simple parabolic band model. However, this model [58] has been shown to be insufficient to explain experiments [59], and has a tendency to significantly overestimate the hole lifetime and to underestimate the electron lifetime [59]. The thermionic lifetime model that we employ in this study is based on the model proposed by Irikawa *et al* [59], that has been applied to the study of 1500 nm InGa(Al)As/InP QW lasers.

The thermionic current leakage, from the edge of the QW to *one side* of the SCH, $J_{\rm ee\_i}$, is related to the thermionic emission carrier lifetime to *one side* of the SCH $\tau_{\rm ee\_i}$ as follows: $J_{\rm ee\_i} = NqL_zN_{\rm QW}/\tau_{\rm ee\_i}$, in which i, N, q, L_z, $N_{\rm QW}$ represent the type of carrier (electrons or holes), the number of QWs, the electron charge, the QW thickness, and the carrier density in the QW, respectively. It is important to note that the thermionic leakage current here is not the same as the total current leakage in QW laser devices, as the carriers leaked into the SCH region will have a probability of being recaptured and recombining in the QW [56, 57, 59]. The relationships of the total threshold current density and the current injection efficiency with the thermionic carrier lifetime are more complex, and are interrelated by the total recombination lifetime in the QW and barrier regions and carrier capture time into the QW [56, 57, 59]. The leakage current $J_{\rm ee\_i}$ has been described in [58, 59] with the standard thermionic emission theory as follows:

$$J_{\rm ee\_i} = \frac{4\pi q(k_{\rm B}T)^2}{h^3} m_i^* \exp\left(-\frac{E_{{\rm b}i} - F_i}{k_{\rm B}T}\right) \tag{5}$$

where m_i^*, $E_{{\rm b}i}$, and F_i are the effective masses of the electrons or holes in the QW and the effective barriers and the quasi-Fermi levels for the electrons or holes in the QW, respectively. $k_{\rm B}$ and h represent the Boltzmann and Planck constants, respectively. The carrier density in the QW is calculated by taking into consideration the 2D DOS of the strained QW, strain effects in the band-gap of the QW, and the Fermi–Dirac statistics [60]. The thermionic escape lifetime ($\tau_{\rm ee\_i}$) can be extracted by relating the thermionic leakage current ($J_{\rm ee\_i}$) and the carrier density in the QW ($N_{\rm QW}$), with consideration of the structure. The *total* current leakage from the single-QW to *both sides* of the SCH, contributed by carrier i (electrons or holes), is $J_{\rm e\_i} = J_{\rm ee\_i\_right} + J_{\rm ee\_i\_left}$. The *total* thermionic escape lifetime of carrier i ($\tau_{\rm e\_i}$) can be expressed as $1/\tau_{\rm e\_i} = 1/\tau_{\rm ee\_i\_right} + 1/\tau_{\rm ee\_i\_left}$. For the case of symmetrical barriers ($J_{\rm ee\_i\_right} = J_{\rm ee\_i\_left}$), the expression $1/\tau_{\rm e\_i} = 2/\tau_{\rm ee\_i}$ will be obtained.

In this study, the $\tau_{\rm ee\_i}$ values are analysed for the case of the 1190 nm emitting InGaAs QW and 1300 nm emitting InGaAsN QW lasers. These 1190–1300 nm InGaAs(N) QW lasers, shown schematically in figure 1, are similar to the lasers that have been reported previously [8, 9], in which a very high In content (∼40%) and minimum N content (∼0.5%) InGaAs(N) QW is utilized to achieve high performance λ = 1190–1300 nm emitting lasers

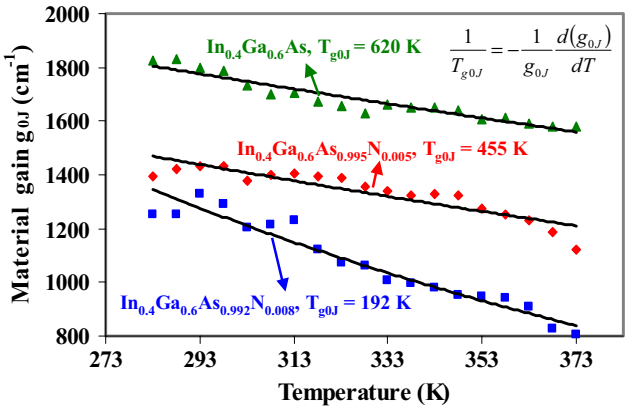

Figure 35. The material gain parameter g_{0J} versus temperature in the range of 10–100 °C. Higher N content results in both lower g_{0J} and lower $T_{g_{0J}}$.

with GaAs as the *direct* barrier to the QW. Large band-gap $Al_{0.74}Ga_{0.26}As$ layers are utilized as the n and p cladding layers, to ensure minimal carrier leakage from the SCH region to the cladding layers. The existence of the small N content (∼0.5–2%) in the InGaAsN QW mainly affects the conduction band, which allows for the approximation of many of the material parameters of the $In_xGa_{1-x}As_{1-y}N_y$ QW by those of the $In_xGa_{1-x}As$ QW [61]. The selection of the parameters used here follows the treatment in [55, 61] for the effective masses of the electrons, band-gap energy, and conduction (ΔE_c) and valence (ΔE_v) band offsets.

We determine the appropriate band offset values by fitting the theory with the *measured* values from the experiments. The conduction band offset ratios ($Q_c = \Delta E_c/\Delta E_g$) for highly strained (In > 20%) InGaAs–GaAs materials have been predicted to be in the range 60–65% [60, 62–64]. For the case of the InGaAsN QW, *experimental* studies [1, 55] show that Q_c is as high as 77–80% for the case of $In_{0.38}Ga_{0.62}As_{0.985}N_{0.015}$. Additional recent work [65] has also demonstrated *experimentally* the reduction in the valence band offset (ΔE_v) in the InGaAsN QW as a result of N incorporation into the InGaAs QW. We found very good agreement in emission wavelength and QW composition between theory and experiment with Q_c values of 65% and 82% for the 63 Å $In_{0.43}Ga_{0.57}As$ QW and 63 Å $In_{0.43}Ga_{0.57}As_{0.9938}N_{0.0062}$ QW, respectively. The compositions, the QW thickness, and the emission wavelengths of the 60 Å $In_{0.4}Ga_{0.6}As$ QW and the 60 Å $In_{0.4}Ga_{0.6}As_{0.995}N_{0.005}$ QW are measured experimentally [8, 24]. m_e^* for the InGaAs QW and InGaAsN QW are calculated here as 0.047 m_0 and 0.069 m_0, respectively, with m_0 the mass of the electron. m_{hh}^* for both InGaAs and InGaAsN QW utilized in the calculation is 0.457 m_0. Due to the large strain of the InGaAs and InGaAsN QW, the hole band structure consists of only heavy hole subbands in the 2D states, with the light hole states having bulk-like (3D) properties.

By utilizing the parameters listed in [58–64] and figure 36, the thermionic escape lifetime τ_{ee_i} can be calculated for electrons and holes for both InGaAs and InGaAsN QWs, as shown in figure 37. For the case of an InGaAs QW, the τ_{ee} (∼50–160 ps) of electrons is comparable to that (∼55–60 ps) of heavy holes, for typical threshold carrier densities of interest ($N_{QW} \sim 1.5$–4×10^{18} cm^{-3}). In the case of an InGaAsN QW, τ_{ee} for the heavy hole is significantly smaller than τ_{ee} for the electron. The electrons are very well confined in the InGaAsN QW, as indicated by the large τ_{ee} (∼40–100 ns) of the electron for typical threshold conditions. This large τ_{ee} for electrons in the InGaAsN QW is expected, owing to

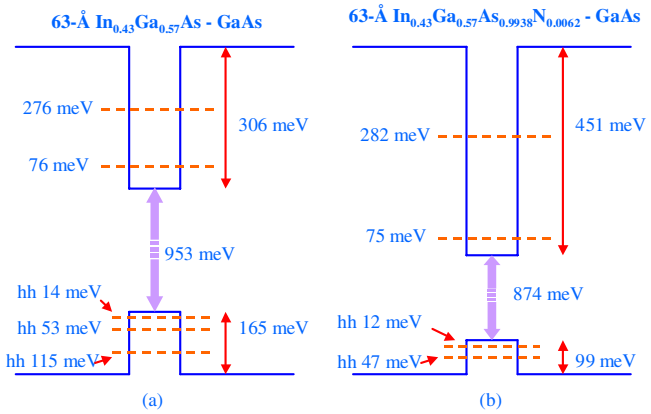

Figure 36. The band line-up for conduction and valence bands of (a) 1190 nm $In_{0.43}Ga_{0.57}As$ QW and (b) 1295 nm $In_{0.43}Ga_{0.57}As_{0.9938}N_{0.0062}$ QW lasers, with GaAs barriers.

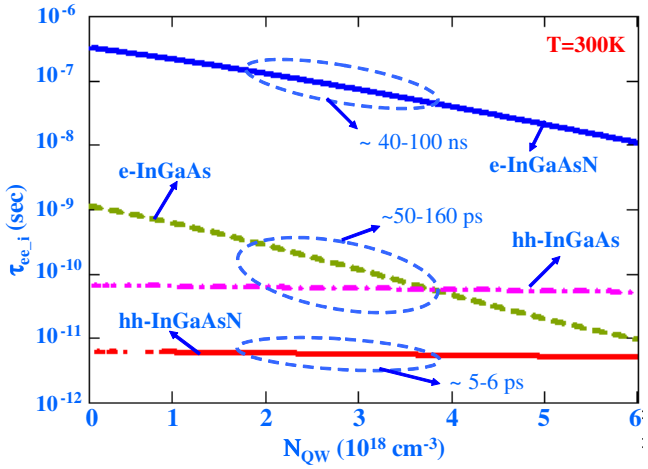

Figure 37. The electron and hole thermionic escape lifetimes of 1190 nm $In_{0.43}Ga_{0.57}As$ QW and 1295 nm $In_{0.43}Ga_{0.57}As_{0.9938}N_{0.0062}$ QW lasers with GaAs barriers, at the temperature of 300 K, as functions of carrier density.

its large conduction band offset ($\Delta E_c \sim 450$ meV). On the other hand, the heavy hole is very poorly confined due to the large disparity of the ΔE_c and ΔE_v. The small valence band offset ($\Delta E_c \sim 99$ meV) in the InGaAsN QW results in a picosecond range τ_{ee} of approximately 5–6 ps, for typical threshold conditions. Due to the significantly smaller τ_{ee} for the hole in the InGaAsN QW, the heavy hole leakage is the dominant leakage mechanism for the InGaAsN QW. Severe thermionic carrier leakage leads to a reduction in the current injection efficiency at threshold [56, 57], which is distinct from the above-threshold η_{inj} [66], and will in turn lead to an increase in the threshold current density of the QW laser.

The thermionic carrier escape lifetimes for the InGaAs and InGaAsN QWs are shown in figures 38(a) and (b). At elevated temperature ($T = 360$ K), τ_{ee} for the heavy hole reduces to only 3 ps. In the case of the InGaAs QW, the lowest τ_{ee} is approximately 21 ps at an elevated temperature of 360 K. The severe heavy hole leakage at elevated temperature for InGaAsN QW lasers serves as one of the contributory factors that leads to the highly temperature

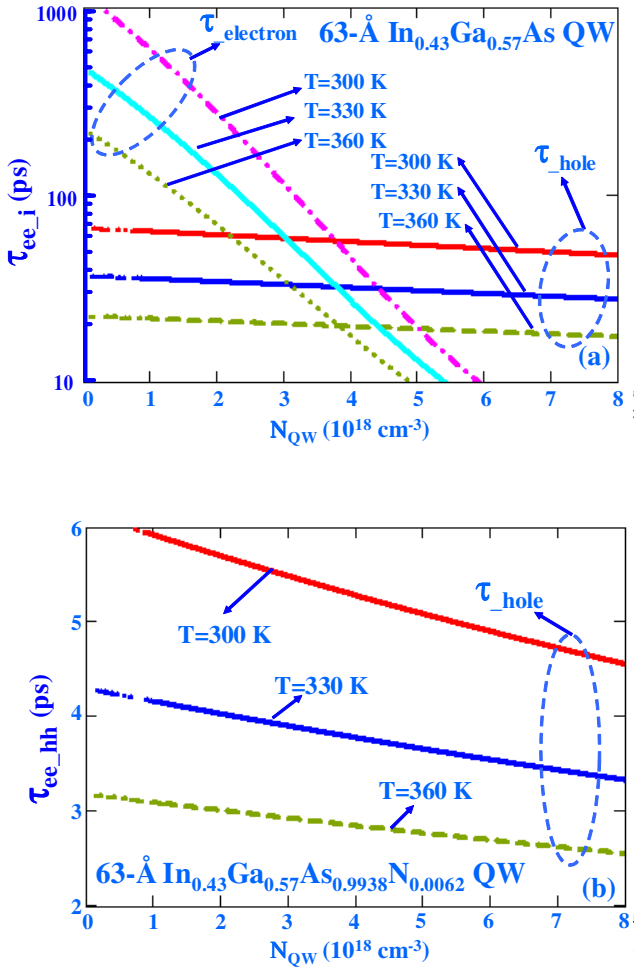

Figure 38. The electron and hole thermionic escape time of the (a) 1190 nm InGaAs QW and (b) the 1295 nm InGaAsN QW lasers with GaAs barriers, as functions of the carrier density and temperature.

sensitive ($T_0 \sim$ 70–90 K) threshold current for high performance 1300 nm InGaAsN QW lasers. Although the hole leakage processes may dominate the high temperature sensitivity of InGaAsN QW lasers, Auger recombination and other processes in the InGaAsN QW cannot be ruled out as contributory factors.

To achieve suppression of hole leakage from the InGaAsN single-QW, larger band-gap materials of tensile GaAsP or InGaAsP can also be utilized as the direct barrier or SCH regions. As shown in figure 39, the τ_{ee} values for holes in an InGaAsN QW were calculated for structures with various barrier regions. By utilizing the 1.77 eV InGaAsP lattice-matched barriers, with the assumption of a band offset ratio (ΔE_c:ΔE_v) of 82:18, the thermionic rate of escape ($1/\tau_{ee\_holes}$) of the heavy holes from the InGaAsN QW is reduced significantly, by approximately 10–12 times, in comparison with that of the InGaAsN–GaAs case. In fact, τ_{ee_holes} (~25 ps, $N_{QW} \sim 3 \times 10^{18}$ cm^{-3}, $T = 360$ K) for the heavy hole for an InGaAsN QW with 1.77 eV barriers at elevated temperature is comparable with the lowest τ_{ee} for carriers in

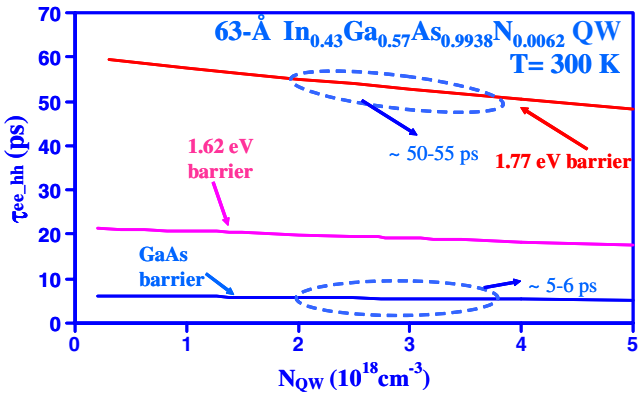

Figure 39. The electron and hole thermionic escape lifetimes of the 1295 nm InGaAsN QW lasers with various barriers, at the temperature of 300 K, as functions of the carrier density.

an InGaAs QW for typical threshold conditions at the same temperature. The utilization of an InGaAsN multiple QW with GaAs barriers is also expected to improve the high temperature laser performance. The utilization of multiple-QW lasers will result in a lower thermionic hole escape rate ($1/\tau_{ee\_holes}$), as $1/\tau_{ee}$ is inversely proportional to the number of QWs (N).

The hole leakage process is identified as the main mechanism in the leakage process in 63 Å $In_{0.43}Ga_{0.57}As_{0.9938}N_{0.0062}$ single-QW lasers with GaAs barriers. At a typical room temperature threshold carrier density ($N_{QW} = 1.5$–3×10^{18} cm^{-3}), the estimated τ_{ee} for the heavy hole in 1300 nm emitting InGaAsN QW lasers is predicted to be around 5–6 ps, which is approximately 10 times smaller than that of the 1190 nm emitting InGaAs QW lasers. Reduction in the hole leakage, achieved by utilizing large band-gap barriers in a single-QW, should allow the realization of high lasing performance and high temperature operation 1300 nm InGaAsN single-QW lasers, comparable to what is achieved with 1190 nm emitting InGaAs single-QW lasers. Utilization of multi-QW InGaAsN active regions will also allow reduction in the thermionic carrier escape rate, which will be beneficial for high temperature operation.

Due to the complexity of determining the parameters for InGaAsN materials, the intent of this section is not to provide the most accurate values of the time for escape of thermionic carriers from InGaAsN QW; rather it is to point out the significance of the thermionic carrier escape processes in 1300 nm InGaAsN QW lasers, which have been neglected in previous analyses under the assumption of strong electron confinement [28]. Further analysis utilizing a self-consistent computation [67], with consideration of thermionic carrier leakage, would allow an improved and more accurate understanding of the physics of the temperature sensitivity of InGaAsN QW lasers.

13. Experimental evidence of the existence of carrier leakages

Our previous studies presented in section 11 have suggested that carrier leakage and a more temperature sensitive material gain are also contributory factors that lead to a stronger temperature sensitivity of the InGaAsN QW lasers in comparison to that of the optimized 1200 nm InGaAs QW lasers. In section 12, we have also calculated theoretically that the thermionic carrier escape rate for 1300 nm InGaAsN QW lasers is larger by one or two orders of magnitude in comparison to that of 1200 nm InGaAs QW lasers, as a result of poor heavy hole confinement in the InGaAsN QW.

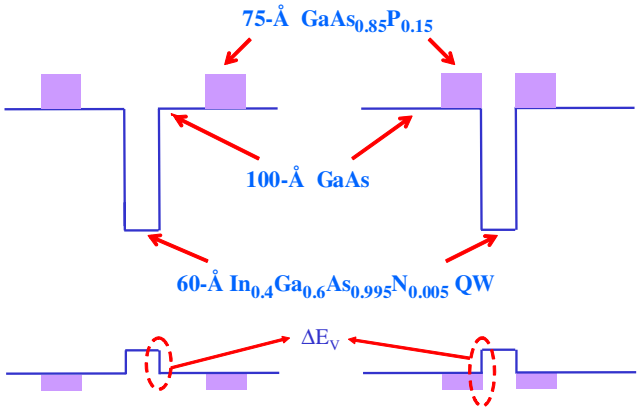

Figure 40. A schematic band diagram of the $In_{0.4}Ga_{0.6}As_{0.995}N_{0.005}$ QW active regions with direct barriers of (a) GaAs and (b) $GaAs_{0.85}P_{0.15}$.

In this section, we describe experimental evidence for the existence of temperature-induced carrier leakage in InGaAsN QW lasers. This work shows experimentally that carrier leakage in InGaAsN QWs cannot be neglected, despite the deep electron confinement. Experiments are designed in which the choice of the barriers surrounding an identical 60 Å $In_{0.4}Ga_{0.6}As_{0.995}N_{0.005}$ QW ($\Delta a/a \sim 2.8\%$, compressive) are modified from the conventional GaAs barriers to higher band-gap ($E_g \sim 1.55$ eV) $GaAs_{0.85}P_{0.15}$ barriers ($\Delta a/a \sim -0.54\%$, tensile), as shown in figure 40. On replacing the direct barrier material, the thermionic escape lifetime of the carriers in the QW will be altered as a consequence of changes in the band offsets (ΔE_b). On utilizing the GaAsP direct barriers, significant suppression of the carrier leakage phenomena at elevated temperature is observed, resulting in the realization of InGaAsN QW lasers with low J_{th} and improved T_0 values at elevated temperatures. It is also important to note that the improvement in T_0 values in the InGaAsN–GaAsP laser structure is not a result of an increase in J_{th}.

J_{th} for QW lasers can be expressed as a function of the device parameters, which include the transparency current density (J_{tr}), current injection efficiency (η_{inj}), material gain parameter (g_{0J}), and internal loss (α_i), as follows [24, 29]:

$$J_{th} = \frac{J_{tr}}{\eta_{inj}} \exp\left(\frac{\alpha_i + (1/L)\ln(1/R)}{\Gamma g_{0J}}\right). \tag{6}$$

η_{inj} is defined as the fraction of the injected current that recombines in the QW active region. An expression for η_{inj} at threshold [56, 57], with the assumption of low photon density (S), can be given as follows:

$$\eta_{inj}(S \to 0) \cong \frac{1}{\left[1 + \frac{\tau_{bw}}{\tau_b}\left(1 + \frac{\tau_{QW\_total}}{\tau_e}\right)\right]}, \tag{7}$$

with τ_{bw} the total carrier transport time, τ_b the total recombination lifetime in the SCH region, τ_{QW_total} the total recombination lifetime in the QW active region, and τ_e the thermionic carrier escape lifetime. Equation (2) can be derived from the conventional rate equation for QW lasers [56, 57]. The τ_{bw} and τ_b are assumed unchanged in all of our experiments, as the design and the choice of material systems for the SCH region are identical for all structures investigated here. From the fact that the compositions and dimensions of the InGaAsN QW active regions in the two experiments are kept identical, the total recombination lifetime in the QW, τ_{QW_total}, can also be assumed unchanged.

The thermionic escape lifetimes ($\tau_{e\_e,h}$ for electrons and holes, respectively) for the carriers in the QW can also be expressed as follows [38, 57, 59]:

$$\frac{1}{\tau_{e\_e,h}} \propto \frac{1}{N_{QW} L_z} T^2 \exp\left(-\frac{\Delta E_{b\_e,h}}{k_B T}\right), \tag{8}$$

with k_B the Boltzmann constant, T the temperature, N_{QW} the carrier density in the QW, L_z the thickness of the QW, and $\Delta E_{b\_e,h}$ the carrier confinement energy in the QW (for electrons and holes, respectively). As the dimensions (L_z) and compositions of the InGaAsN QW active regions in the two experiments are identical, the threshold carrier densities in the QWs (N_{QW_th}) can also be assumed identical for the two lasers with similar confinement and cladding layer designs. The total thermionic carrier escape time for the QW (τ_e) can be expressed as a function of $\tau_{e\_electron}$ and τ_{e_holes}, as $1/\tau_e = 1/\tau_{e\_electron} + 1/\tau_{e\_holes}$. The escape phenomenon is dominated by the escape rate of the carriers with the fastest escape time. Once the carriers escape, the carriers in the QW and SCH will redistribute themselves to maintain charge neutrality in the QW and SCH due to the high mobility of the carriers [56]. The difference between the τ_e values of the InGaAsN–GaAs and InGaAsN–GaAsP structures can be attributed solely to the difference between their respective ratios $\Delta E_{b\_e,h}/k_B T$. The ratios of the electron and hole confinement energies (ΔE_c:ΔE_v, with $\Delta E_c = \Delta E_{b\_e}$, $\Delta E_v = \Delta E_{b\_h}$) in InGaAsN–GaAs structures, is approximately 80:20 [38, 55], resulting in extremely strong electron confinement and extremely poor heavy hole confinement. The calculated escape lifetimes for the electrons and holes in the InGaAsN QW are approximately 30–50 ns and 5–10 ps, respectively, for near threshold conditions [38]. By utilizing the large band-gap material surrounding the InGaAsN QW, the confinement energy will be increased for both the electrons and the holes in the QW. As no study has been reported on the InGaAsN–GaAsP structures, the ΔE_c:ΔE_v ratio is assumed similar to that of the InGaAsN–GaAs case. A calculated increase in ΔE_v (without taking into account the tensile strain of GaAsP) of approximately 22–35 meV can be achieved for the InGaAsN–GaAsP structures, which is approximately 25% larger than that for InGaAsN–GaAs structures ($\Delta E_v \sim 99$ meV [38]). Slight increase in ΔE_v leads to significant suppression of the rate of hole escape ($1/\tau_e$) from the InGaAsN–GaAsP QW structures due to its exponential relation (from equation (8)), which will in turn lead to improved η_{inj} and J_{th} at elevated temperatures (from equations (6) and (7)). In the absence of any carrier leakage, by contrast, increase in ΔE_v will not lead to any reduction in J_{th} at elevated temperatures or any improvement in the T_0 values. The tensile strain of the GaAsP barriers could potentially lead to even further improved confinement of heavy holes in the InGaAsN QW, due to the strain-induced lowering of the heavy hole band edge of the tensile strain material.

The laser structures studied here, shown in figure 40, were grown and fabricated by similar methods, as described in sections 2, 3, and 4. The detail of the MOCVD growth of InGaAsN QW materials utilizing GaAs barriers and larger band-gap materials of GaAsP has been discussed elsewhere, in [13] and [68].

As-cleaved broad area lasers, with oxide-defined stripe width of 100 μm, were fabricated for both active regions shown in figure 40. The lasing characteristics were measured under pulsed conditions with a pulse width and a duty cycle of 5 μs and 1%, respectively. Room temperature threshold current densities of 320, 260, and 220 A cm^{-2} were measured for InGaAsN–GaAsP QW lasers for cavity lengths of 775, 1000, and 2000 μm, respectively. At room temperature ($T = 20\,^{\circ}$C), the threshold characteristics of both the InGaAsN–GaAs lasers are measured as approximately 350–360, 250, and 210–220 A cm^{-2}, for devices with cavity lengths of 720, 1000, and 2000 μm, respectively. The emission wavelength of the InGaAsN–GaAsP lasers is approximately 1280 nm ($L_{cav} = 2000\,\mu$m), which is approximately

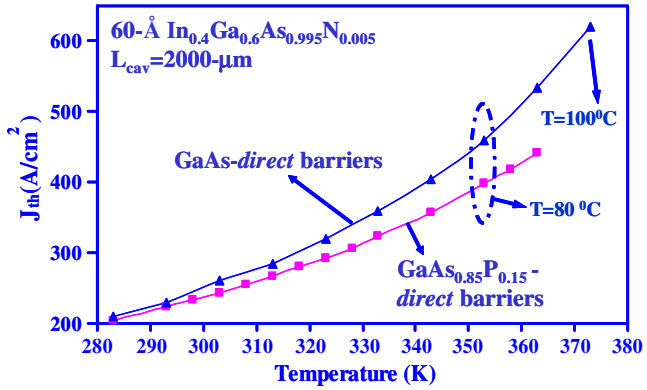

Figure 41. The measured threshold current densities of InGaAsN–GaAs QW and InGaAsN–GaAsP QW lasers as a function of temperature, for the as-cleaved situation, with $L_{\mathrm{cav}} = 2000\ \mu$m.

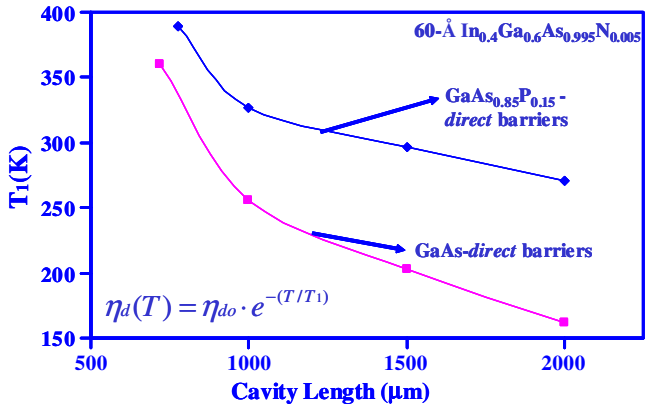

Figure 42. The comparison of the T_1 values, measured for temperatures of 10–60 °C, for $In_{0.4}Ga_{0.6}As_{0.995}N_{0.005}$ QW lasers with $GaAs_{0.85}P_{0.15}$ barriers and GaAs barriers, for various cavity lengths.

150 Å shorter than that of the InGaAsN–GaAs QW structures. Calculations considering the band-gap, strain, and effective masses predict a blue-shift of the emission wavelength of approximately 100–120 Å for InGaAsN–GaAsP QW structures, in good agreement with experiments.

The temperature characterizations of both InGaAsN–GaAsP and InGaAsN–GaAs QW lasers are performed over the range of 10–100 °C. The characteristics of J_{th} with temperature for both laser structures ($L_{\mathrm{cav}} = 2000\ \mu$m) are plotted in figure 41. The measurement is conducted for devices with long cavities to minimize the effect from the temperature sensitivity of the material gain [24, 29]. The threshold current densities of the two lasers are nearly identical in the temperature region below 20 °C. As the temperature increases, J_{th} for the InGaAsN with GaAsP barriers increases at a significantly slower rate. Suppression of the carrier leakage is also evident from the fact that the T_0 and T_1 ($1/T_1 = -(1/\eta_{\mathrm{d}})\,\mathrm{d}\eta_{\mathrm{d}}/\mathrm{d}T$, η_{d} = external differential quantum efficiency) values of the InGaAsN–GaAsP structures are significantly improved for devices with various cavity lengths, as shown in figures 42 and 43. Threshold current densities of only 390 and 440 A cm^{-2} were also measured for InGaAsN–

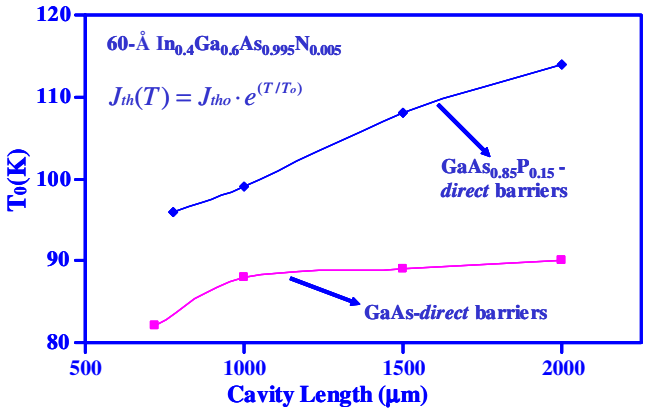

Figure 43. The comparison of the T_0 values, measured for temperatures of 10–60 °C, for $In_{0.4}Ga_{0.6}As_{0.995}N_{0.005}$ QW lasers with $GaAs_{0.85}P_{0.15}$ barriers and GaAs barriers, for various cavity lengths.

GaAsP QW lasers ($L_{cav} = 2000\ \mu$m) at temperatures of 80 and 90 °C, respectively. As electrons are very well confined in both InGaAsN QW laser structures, the reduction of J_{th} for the InGaAsN–GaAsP QW structures at elevated temperatures as well as their improved T_0 and T_1 values are results of the suppression of the heavy hole leakage from the InGaAsN QW due to the lower hole escape rate $(1/\tau_{e\_hole})$.

The existence of carrier leakage in InGaAsN QW lasers has been demonstrated experimentally as one of the contributory factors influencing the temperature sensitivity of InGaAsN lasers. It is important to note that while these experiments demonstrate the existence of carrier leakage processes in InGaAsN QW lasers, they do not rule out Auger recombination as an additional contributory factor in the device temperature sensitivity. Suppression of carrier leakage in InGaAsN QW lasers with larger band-gap barrier material GaAsP leads to a reduction in J_{th} at elevated temperature, accompanied by increases in the T_0 and T_1 values. J_{th} for the InGaAsN QW lasers ($L_{cav} = 2000\ \mu$m, as-cleaved), with $GaAs_{0.85}P_{0.15}$ direct barriers, has been measured as *only* 220 and 390 A cm^{-2}, for measurements at temperatures of 20 and 80 °C, respectively.

14. Conclusions

High performance InGaAs and InGaAsN QWs lasers, with emission wavelengths ranging from 1170 to 1320 nm, have been realized by MOCVD growth using AsH_3 as the As precursor. Low threshold current density and high temperature operation was obtained for 1300 nm InGaAsN single-QW lasers, resulting in superior performance in comparison to that of conventional 1300 nm InP-based lasers. Despite the high strain of the InGaAsN QW, multiple-QW lasers have been demonstrated with excellent scaling in transparency current and material gain. The utilization of a higher N content InGaAsN QW has indicated possible increased carrier leakage, in comparison to the structures with lower N content InGaAsN QW active regions. Remaining issues concern the reliability of these active layer materials as well as the extension to longer wavelengths. In addition to the success of the 1300 nm InGaAsN QW lasers, we have demonstrated excellent lasing characteristics for InGaAsN QW lasers within the emission wavelength range of 1360–1382 nm, by utilizing MOCVD with AsH_3 as the As precursor. These results represent among the lowest reported threshold current densities for InGaAsN

QW lasers for emission wavelengths of 1360 and 1382 nm. We observe a strong dependence of the device temperature sensitivity (T_0 and T_1) on the nitrogen content of the QW. The reasonably low J_{th} values of the 1360 and 1382 nm InGaAsN QW lasers also indicate the feasibility of pushing the InGaAsN QW technology beyond the emission wavelength of 1400 nm.

Detailed analysis of the temperature characteristics of InGaAsN QW lasers indicated the importance of suppression of thermionic carrier leakage to realize low threshold lasers. Here we have calculated theoretically and demonstrated experimentally that by suppressing the carrier leakage out of the InGaAsN QW, high performance lasers can be realized up to very high temperature.

Acknowledgments

The authors would like to acknowledge helpful technical discussions with Drs M R T Tan, D P Bour, S W Corzine, T Takeuchi, Y L Chang (Agilent Technologies Laboratories, Palo Alto, CA).

References

[1] Kondow M, Kitatani T, Nakatsuka S, Larson M C, Nakahara K, Yazawa Y, Okai M and Uomi K 1997 GaInNAs: a novel material for long wavelength semiconductor lasers *IEEE J. Sel. Top. Quantum Electron.* **3** 719–30

[2] Harris J S Jr 2000 Tunable long-wavelength vertical-cavity lasers: the engine of next generation optical networks? *IEEE J. Sel. Top. Quantum Electron.* **6** 1145–60

[3] Sato S 2000 Low threshold and high characteristics temperature 1.3 μm range GaInNAs lasers grown by metal–organic chemical vapor deposition *Japan. J. Appl. Phys.* **39** 3403–5

[4] Livshits D A, Egorov A Yu and Riechert H 2000 8 W continuous wave operation of InGaAsN lasers at 1.3 μm *Electron. Lett.* **36** 1381–2

[5] Hohnsdorf F, Koch J, Leu S, Stolz W, Borchert B and Druminski M 1999 Reduced threshold current densities of (GaIn)(NAs)/GaAs single quantum well lasers for emission wavelengths in the range 1.28–1.38 μm *Electron. Lett.* **35** 571–2

[6] Kawaguchi M, Miyamoto T, Gouardes E, Schlenker D, Kondo T, Koyama F and Iga K 2001 Lasing characteristics of low-threshold GaInNAs lasers grown by metal–organic chemical vapor deposition *Japan. J. Appl. Phys.* **40** L744–6

[7] Takeuchi T, Chang Y-L, Leary M, Tandon A, Luan H-C, Bour D P, Corzine S W, Twist R and Tan M R 2001 Low threshold 1.3 μm InGaAsN vertical cavity surface emitting lasers grown by metal–organic chemical vapor deposition *IEEE LEOS 2001 Post-Deadline Session (San Diego, CA. Nov. 2001)* (Piscataway, NJ: IEEE)

[8] Tansu N and Mawst L J 2002 Low-threshold strain-compensated InGaAs(N) ($\lambda = 1.19$–1.31 μm) quantum well lasers *IEEE Photon. Technol. Lett.* **14** 444–6

[9] Tansu N, Kirsch N J and Mawst L J 2002 Low-threshold-current-density 1300 nm dilute-nitride quantum well lasers *Appl. Phys. Lett.* **81** 2523–5

[10] Tansu N, Quandt A, Kanskar M, Mulhearn W and Mawst L J 2003 High-performance and high-temperature continuous-wave-operation 1300 nm InGaAsN quantum well lasers by organometallic vapor phase epitaxy *Appl. Phys. Lett.* **83** 18–20

[11] Tansu N, Yeh J Y and Mawst L J 2003 Experimental evidence of carrier leakage in InGaAsN quantum-well lasers *Appl. Phys. Lett.* **83** 2112–4

[12] Tansu N, Yeh J Y and Mawst L J 2003 Low-threshold 1317 nm InGaAsN quantum well lasers with GaAsN barriers *Appl. Phys. Lett.* **83** 2512–4

[13] Tansu N, Yeh J Y and Mawst L J 2003 Improved photoluminescence of InGaAsN–(In)GaAsP quantum well by organometallic vapor phase epitaxy using growth pause annealing *Appl. Phys. Lett.* **82** 3008–110

[14] Tansu N, Yeh J Y and Mawst L J 2003 High-performance 1200 nm InGaAs and 1300 nm InGaAsN quantum-well lasers by metal–organic chemical vapor deposition *IEEE J. Sel. Top. Quantum Electron.* **3** 1220–7

[15] Wei J, Xia F, Li C and Forrest S R 2002 High T_0 long-wavelength InGaAsN quantum-well lasers grown by GSMBE using a solid arsenic source *IEEE Photon. Technol. Lett.* **14** 597

[16] Choquette K D *et al* 2000 Room temperature continuous wave InGaAsN quantum well vertical-cavity lasers emitting at 1.3 μm *Electron. Lett.* **36** 1388–90

[17] Ha W, Gambin V, Wistey M, Bank S, Kim S and Harris J S Jr 2002 Multiple quantum well GaInNAs–GaNAs ridge-waveguide laser diodes operating out to 1.4 μm *IEEE Photon. Technol. Lett.* **14** 591–3
[18] Peng C S, Jouhti T, Laukkanen P, Pavelescu E-M, Konttinen J, Li W and Pessa M 2002 1.32 μm GaInNAs–GaAs laser with a low threshold current density *IEEE Photon. Technol. Lett.* **14** 275–7
[19] Li W, Jouhti T, Peng C S, Konttinen J, Laukkanen P, Pavelescu E-M and Pessa M 2001 Low-threshold-current 1.32 μm GaInNAs–GaAs single-quantum-well lasers grown by molecular-beam epitaxy *Appl. Phys. Lett.* **79** 3386–8
[20] Sato S and Satoh S 1999 1.21 μm continuous-wave operation of highly strained GaInAs quantum well lasers on GaAs substrates *Japan. J. Appl. Phys.* **38** L990–2
[21] Choi W, Dapkus D P and Jewell J J 1999 1.2 μm GaAsP/InGaAs strain compensated single-quantum well diode laser on GaAs using metal–organic chemical vapor deposition *IEEE Photon. Technol. Lett.* **11** 1572–4
[22] Kondo T, Schlenker D, Miyamoto T, Chen Z, Kawaguchi M, Gouardes E, Koyama F and Iga K 2000 Lasing characteristics of 1.2 μm highly strained GaInAs/GaAs quantum well lasers *Japan. J. Appl. Phys.* **40** 467–71
[23] Tansu N and Mawst L J 2001 High-performance, strain compensated InGaAs–GaAsP–GaAs ($\lambda = 1.17$ μm) quantum well diode lasers *IEEE Photon. Technol. Lett.* **13** 179–81
[24] Tansu N, Chang Y L, Takeuchi T, Bour D P, Corzine S W, Tan M R T and Mawst L J 2002 Temperature analysis and characteristics of highly-strained InGaAs(N)–GaAs–InGaP ($\lambda > 1.17$ μm) quantum well lasers *IEEE J. Quantum Electron.* **38** 640–51
[25] Tansu N, Yeh J Y and Mawst L J 2003 Extremely low threshold-current-density InGaAs quantum-well lasers with emission wavelength of 1215–1233 nm *Appl. Phys. Lett.* **82** 4038–40
[26] Takeuchi T, Chang Y-L, Tandon A, Bour D, Corzine S, Twist R, Tan M and Luan H-C 2002 Low threshold 1.2 μm InGaAs quantum well lasers grown under low As/III ratio *Appl. Phys. Lett.* **80** 2445–7
[27] Bugge F, Erbert G, Fricke J, Gramlich S, Staske R, Wenzel H, Zeimer U and Weyers M 2001 12 W continuous-wave diode lasers at 1120 nm with InGaAs quantum wells *Appl. Phys. Lett.* **79** 1965–7
[28] Fehse R, Tomic S, Adams A R, Sweeney S J, O'Reilly E P, Andreev A and Riechert H 2002 A quantitative study of radiative, auger, and defect related recombination processes in 1.3 μm GaInNAs-based quantum-well lasers *IEEE Sel. J. Quantum Electron.* **8** 801–10
[29] Tansu N and Mawst L J 2002 Temperature sensitivity of 1300 nm InGaAsN quantum well lasers *IEEE Photon. Technol. Lett.* **14** 1052–4
[30] Tansu N and Mawst L J 2004 Temperature-sensitivity analysis of 1360 nm dilute-nitride quantum well lasers *IEEE Photon. Technol. Lett.* **16** 741–3
[31] Chen Z B, Schlenker D, Koyama F, Miyamoto T, Matsutani A and Iga K 1999 High temperature characteristics of highly strained 1.2 μm InGaAs/GaAs lasers *Proc. APCC/OECC'99 (Beijing, China, 1999)* vol 2, pp 1311–4
[32] Mogg S, Chitica N, Schatz R and Hammar M 2002 Properties of highly strained InGaAs/GaAs quantum wells for 1.2 μm laser diodes *Appl. Phys. Lett.* **81** 2334–6
[33] Sellin R L, Ribbat Ch, Grundmann M, Ledentsov N N and Bimberg D 2001 Close-to-ideal device characteristics of high-power InGaAs/GaAs quantum dot lasers *Appl. Phys. Lett.* **78** 1207–9
[34] Stintz A, Liu G T, Li H, Lester L F and Malloy K J 2000 Low-threshold current density 1.3 μm quantum-dot lasers with the dots-in-a-well (DWELL) structure *IEEE Photon. Technol. Lett.* **12** 591–3
[35] Smowton P M, Hermann E, Ning Y, Summers H D and Blood P 2001 Optical mode loss and gain of multiple-layer quantum-dot lasers *Appl. Phys. Lett.* **78** 2629–31
[36] Belenky G L *et al* 1999 *IEEE J. Quantum Electron.* **35** 1515
[37] Savolainen P *et al* 1999 *Proc. 11th IPRM 1999,* Paper MoP09
[38] Tansu N and Mawst L J 2003 The role of hole-leakage in 1300 nm InGaAsN quantum well lasers *Appl. Phys. Lett.* **82** 1500–2
[39] Wu J, Shan W, Walukiewicz W, Yu K M, Ager J W III, Haller E E, Xin H P and Tu C W 2001 *Phys. Rev.* B **64** 85320
[40] Sun B Q, Jiang D S, Luo X D, Xu Z Y, Pan Z, Li L H and Wu R H 2000 *Appl. Phys. Lett.* **76** 2862
[41] Kitatani T, Kondow M, Kikawa T, Yazawa Y, Okai M and Uomi K 1999 *Japan. J. Appl. Phys.* **38** 5003
[42] Illek S, Ultsch A, Borchert B, Egorov A Y and Riechert H 2000 Low threshold lasing operation of narrow stripe oxide-confined GaInNAs/GaAs multiquantum well lasers at 1.28 μm *Electron. Lett.* **36** 725–6
[43] Fischer M, Reinhardt M and Forchel A 2000 High temperature operation of GaInAsN laser diodes in the 1.3 μm regime *Device Research Conf. (June 2000)* pp 19–21
[44] Borchert B, Egorov A Y, Illek S, Komainda M and Riechert H 1999 1.29 μm GaInNAs multiple quantum-well ridge-waveguide laser diodes with improved performance *Electron. Lett.* **35** 2204–6
[45] Sato S and Satoh S 1999 High-temperature characteristic in 1.3 μm-range highly strained GaInNAs ridge stripe lasers grown by metal–organic chemical vapor deposition *IEEE Photon. Technol. Lett.* **11** 1560–2

[46] Nakahara K, Kondow M, Kitatani T, Larson M C and Uomi K 1998 1.3 μm continuous-wave lasing operation in GaInNAs quantum-well lasers *IEEE Photon. Technol. Lett.* **10** 487–8
[47] Thijs P J A, Tiemeuer L F, Binsma J J M and Van Dongen T 1994 Progress in long-wavelength strained-layer InGaAs(P) quantum-well semiconductor lasers and amplifiers *IEEE J. Quantum Electron.* **30** 477–99
[48] Yokouchi N, Yamanaka N, Iwai N and Kasukawa A 1995 Low threshold 1.3 μm-GaInAsP–InP tensile strained single quantum well lasers grown by low-pressure MOCVD *Electron. Lett.* **31** 104–5
[49] Donnelly J P, Groves S H, Walpole J N, Bailey R J, Woodhouse J D, Missaggia L J, Napoleone A, O'Donnell F J and Reeder R E 1994 Low-transparency-current-density, high-gain 1.3 μm strained-layer InGaAsP/InP quantum-well laser material *Conf. Proc. LEOS 1994 (Oct. 1994)* vol 2, pp 406–7
[50] Zah C E *et al* 1994 High-performance uncooled 1.3 μm $Al_xGa_yIn_{1-x-y}As$/InP strained-layer quantum-well lasers for subscriber loop applications *IEEE J. Quantum Electron.* **30** 511–23
[51] Selmic S R, Chou T-M, Sih J, Kirk J B, Mantle A, Butler J K, Bour D and Evans G A 2001 Design and characterization of 1.3 μm AlGaInAs–InP multiple-quantum-well lasers *IEEE J. Sel. Top. Quantum Electron.* **7** 340–9
[52] Takeuchi T, Chang Y-L, Leary M, Tandon A, Luan H-C, Bour D P, Corzine S W, Twist R and Tan M R 2003 *Proc. SPIE Photonics West 2003, Novel In-Plane Semiconductor Lasers 2003 (San Jose, CA, Jan. 2003)* Paper 4995-08
[53] Fischer M, Reinhardt M and Forchel A 2000 *Electron. Lett.* **36** 1204
[54] Ikenaga Y, Miyamoto T, Makino S, Kageyama T, Arai M, Koyama F and Iga K 2002 *Japan. J. Appl. Phys.* **41** 665
[55] Hetterich M, Dawson M D, Egorov A Yu, Bernklau D and Riechert H 2000 Electronic states and band alignment in GaInNAs/GaAs quantum-well structures with low nitrogen content *Appl. Phys. Lett.* **76** 1030–2
[56] Nagarajan R and Bowers J E 1993 *IEEE. J. Quantum Electron.* **29** 1601
[57] Tansu N and Mawst L J 2004 unpublished
[58] Schneider H and Klitzing K V 1988 *Phys. Rev.* B **38** 6160
[59] Irikawa M, Ishikawa T, Fukushima T, Shimizu H, Kasukawa A and Iga K 2000 *Japan. J. Appl. Phys.* **39** 1730
[60] Chuang S L 1995 *Physics of Optoelectronic Devices* (New York: Wiley)
[61] Chow W W, Jones E D, Modine N A, Allerman A A and Kurtz S R 1999 *Appl. Phys. Lett.* **75** 2891
[62] Jogai B 1991 *Appl. Phys. Lett.* **59** 1329
[63] Coleman J J 1993 *Quantum Well Lasers* ed P S Zory (New York: Academic) chapter 8
[64] Niki S, Lin C L, Chang W S C and Wieder H H 1989 *Appl. Phys. Lett.* **55** 1339
[65] Heroux J B, Yang C and Wang W I 2002 *J. Appl. Phys.* **92** 4361
[66] Smowton P M and Blood P 1997 *IEEE J. Sel. Top. Quantum Electron.* **3** 491
[67] Piprek J, Abraham P and Bowers J E 2000 *IEEE J. Quantum Electron.* **36** 366
[68] Yeh J Y, Tansu N and Mawst L J 2004 *J. Cryst. Growth* **265** (1-2) 1–7
[69] Sung L W and Lin H H 2003 *Appl. Phys. Lett.* **83** 1107